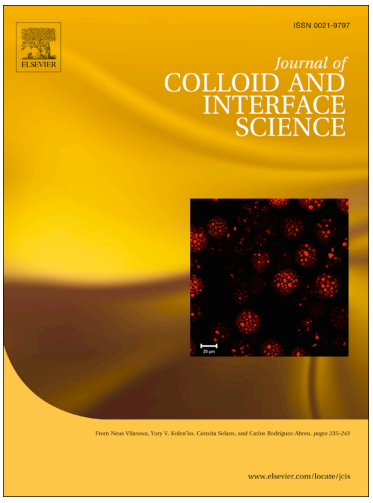

Synthesis and application of sugarcane bagasse cellulose mixed esters. Part I: Removal of Co^{2+} and Ni^{2+} from single spiked aqueous solutions in batch mode using sugarcane bagasse cellulose succinate phthalate

Megg Madonyk Cota Elias, Gabriel Max Dias Ferreira, Francine Tatiane Rezende de Almeida, Nathália Cristina Martins Rosa, Isabela Almeida Silva, Jefferson Gonçalves Filgueiras, Eduardo Ribeiro de Azevedo, Luis Henrique Mendes da Silva, Tânia Márcia Sacramento Melo, Laurent Frédéric Gil, Leandro Vinícius Alves Gurgel

PII: S0021-9797(18)31032-4
DOI: https://doi.org/10.1016/j.jcis.2018.08.109
Reference: YJCIS 24042

To appear in: *Journal of Colloid and Interface Science*

Received Date: 21 May 2018
Accepted Date: 29 August 2018

Please cite this article as: M.M.C. Elias, G.M.D. Ferreira, F.T.R. de Almeida, N.C.M. Rosa, I.A. Silva, J.G. Filgueiras, E.R. de Azevedo, L.H.M. da Silva, T.M.S. Melo, L.F. Gil, L.V.A. Gurgel, Synthesis and application of sugarcane bagasse cellulose mixed esters. Part I: Removal of Co^{2+} and Ni^{2+} from single spiked aqueous solutions in batch mode using sugarcane bagasse cellulose succinate phthalate, *Journal of Colloid and Interface Science* (2018), doi: https://doi.org/10.1016/j.jcis.2018.08.109

Synthesis and application of sugarcane bagasse cellulose mixed esters. Part I: Removal of Co^{2+} and Ni^{2+} from single spiked aqueous solutions in batch mode using sugarcane bagasse cellulose succinate phthalate

Megg Madonyk Cota Elias[a], Gabriel Max Dias Ferreira[a], Francine Tatiane Rezende de Almeida[a], Nathália Cristina Martins Rosa[a], Isabela Almeida Silva[b], Jefferson Gonçalves Filgueiras[b], Eduardo Ribeiro de Azevedo[b], Luis Henrique Mendes da Silva[c], Tânia Márcia Sacramento Melo[a], Laurent Frédéric Gil[a], Leandro Vinícius Alves Gurgel[a,*]

[a] Grupo de Físico-Química Orgânica, Departamento de Química, Instituto de Ciências Exatas e Biológicas, Universidade Federal de Ouro Preto, Campus Morro do Cruzeiro, s/n°, Bauxita, 35400-000 Ouro Preto, Minas Gerais, Brazil

[b] Departamento de Física e Ciência Interdisciplinar, Instituto de Física de São Carlos, Universidade de São Paulo, Av. Trabalhador São-carlense, 400, 13566-590 São Carlos, São Paulo, Brazil

[c] Grupo de Química Verde Coloidal e Macromolecular, Departamento de Química, Centro de Ciências Exatas e Tecnológicas, Universidade Federal de Viçosa, Av. P. H. Rolfs, s/n°,36570-000 Viçosa, Minas Gerais, Brazil

*Corresponding author. Tel.: +55 31 3559 1744; fax + 55 31 3559 1707; E-mail addresses: legurgel@iceb.ufop.br, legurgel@yahoo.com.br (L.V.A Gurgel)

Abstract

Sugarcane bagasse cellulose mixed ester succinate phthalate (SBSPh) was synthesized by a novel one-pot reaction method. The effects of temperature, time and mole fraction of succinic anhydride (χ_{SA}) on the responses weight gain (*wg*), number of carboxylic acid groups ($n_{T,COOH}$), and adsorption capacity (q) of Co^{2+} and Ni^{2+} were evaluated by a 2^3 experimental design. The chemical structure of the material was elucidated by Fourier transform infrared, ^{13}C Multiple Cross-Polarization solid-state NMR spectroscopies and ^{1}H NMR relaxometry. The best SBSPh synthesis condition (100 °C, 11 h, χ_{SA} of 0.2) yielded a *wg* of 59.1%, $n_{T,COOH}$ of 3.41 mmol g^{-1}, and values of $q_{Co^{2+}}$ and $q_{Ni^{2+}}$ of 0.348 and 0.346 mmol g^{-1}, respectively. The Sips model fitted better the equilibrium data, and the maximum adsorption capacities (pH 5.75 and 25 °C) estimated by this model were 0.62 and 0.53 mmol g^{-1} for Co^{2+} and Ni^{2+}, respectively. The $\Delta_{ads}H°$ values estimated by isothermal titration calorimetry were 8.43 and 7.79 kJ mol^{-1} for Co^{2+} and Ni^{2+}, respectively. Desorption and re-adsorption efficiencies were evaluated by a 2^2 experimental design, which showed that SBSPh adsorbent can be recovered and reused without significant loss of adsorption capacity.

Keywords: Mixed esters; sugarcane bagasse; ^{13}C Multiple Cross-Polarization solid-state NMR; metal ion; adsorption; isothermal titration calorimetry

1. Introduction

Heterosubstituted cellulose mixed esters are of particular interest in the development of materials with unique properties. The introduction of two or more types of acyl (aliphatic and aromatic) groups to the same cellulose backbone gives additional properties when compared to the homosubstituted cellulose esters [1]. The growing demand for more specific applications of materials based on renewable resources, such as lignocellulose materials [2], increases the interest in more diversified synthesis pathways [3] along with the design of new derivatives with more than one functional group [4].

An important technological application of modified lignocellulose materials is in the control of water pollution [5, 6]. Clean water is an important matter in the modern society facing environmental problems such as pollution of water resources and progressive reduction in freshwater availability [7]. In addition, water scarcity impairs the life quality of the population and the implementation of new industries due to water supply constraints [8]. Fortunately, many recent scientific studies are finding the answer in naturally occurring biopolymers such as lignocellulose materials. Non-modified and modified lignocellulose materials continue to impact water treatment significantly because of their physicochemical properties, various applications, and cost-effective [5, 6, 9, 10]. However, to the best of our knowledge, chemical modification of lignocellulose materials with two cyclic carboxylic acid anhydrides in a one-pot reaction has not yet been reported. The adsorption properties of an adsorbent can be modulated by the type of carboxylic acid anhydride used in the chemical modification [11, 12], thereby adding more specific and desirable properties to the lignocellulose material for a wide range of applications.

In the first part of this series of studies, the synthesis of a sugarcane bagasse cellulose mixed ester succinate phthalate (SBSPh) was evaluated by a design of experiments using a novel one-pot synthesis method. A complete characterization of the structure of SBSPh was performed by Fourier transform infrared, ^{13}C Multiple Cross-Polarization (Multi-CP) solid-state NMR spectroscopies and ^{1}H NMR relaxometry. The aim of this study was also to prepare an adsorbent material with better adsorption properties, combining the characteristics of the carboxylic groups of aliphatic and aromatic moieties. The effects of temperature, time and mole fraction of succinic anhydride on the responses weight gain, total number of carboxylic acid groups introduced, and adsorption capacity of Co^{2+} and Ni^{2+} were evaluated, aiming at an environmental application of the novel synthesized material in water treatment. Adsorption of both metal ions as a function of solution pH, kinetics and isotherm was also optimized. Studies of desorption and re-adsorption were carried out, and desorption, regeneration and reuse of the adsorbent material were evaluated by design of experiments. The enthalpy of adsorption was also assessed by isothermal titration calorimetry and the adsorption discussed based on thermodynamic parameters obtained.

2. Material and methods

2.1. Material

Phthalic (MW = 148.12 g mol^{-1}) and succinic (MW = 100.07 g mol^{-1}) anhydrides, *N*,*N*-dimethylacetamide (chromatographic grade), $CH_2ClCOOH$ and $CH_2ClCOONa$ were purchased from Sigma-Aldrich. Pyridine (Py), cyclohexane, absolute ethanol, $CaCl_2$, NaOH, HCl (37 wt % in water), HNO_3, glacial acetic acid, $CH_3COONa{\cdot}3H_2O$, $CoCl_2{\cdot}6H_2O$, and $CuSO_4{\cdot}5H_2O$ were purchased from Synth (Brazil). $NaNO_3$ was purchased from Reagen (Brazil). Quantitative filter papers (black ribbon, JP-41,

12.5 cm diameter, ash content 0.00009 g, grammage of 80 g m^{-2}) were purchased from JProlab (Brazil). The adsorption studies were performed using buffer solutions consisting of 0.05 mol L^{-1} $CH_2ClCOOH/CH_2ClCOONa$ (pH from 2.0 to 3.5) and CH_3COOH/CH_3COONa (pH from 4.0 to 5.75). All aqueous solutions were prepared in deionized water (Millipore, model Milli-Q®). Sugarcane bagasse (SB) was provided by Jatiboca Sugar and Ethanol Plant (Urucânia, MG, Brazil). SB was prepared for chemical modification according to the methodology reported by Ramos et al. [12].

2.2. Characterization of sugarcane bagasse

The composition of SB in terms of cellulose, hemicelluloses and lignin was determined using the following standard methods: "Solvent Extractives of Wood and Pulp", TAPPI T204 cm-07, "Acid-insoluble Lignin in Wood and Pulp", TAPPI T222 om-02, "Determination of Acid-soluble Lignin in Biomass", NREL LAP-004, and "Determination of Carbohydrates in Biomass by High Performance Liquid Chromatography", NREL LAP-002. Calculation of the contents of cellulose, hemicelluloses and lignin and other equipment and methods used were those reported by Baêta et al. [13] and Lima et al. [14].

2.3. Synthesis of sugarcane bagasse cellulose succinate phthalate

The synthesis of sugarcane bagasse cellulose succinate phthalate (SBSPh), schematized in Figure 1, was evaluated by a 2^3 experimental design. The typical procedure used in the one-pot synthesis of SBSPh was as follows: 1.000 g of SB and different amounts of phthalic (PA) and succinic (SA) anhydrides were weighed into a 50 mL round-bottomed flask to give an anhydride-to-SB ratio of 4.0 g g^{-1}. Then, 15 mL of anhydrous pyridine was added to give a solvent-to-SB ratio of 15 mL g^{-1}. The flask was equipped with a reflux condenser attached to a drying tube packed with anhydrous calcium chloride

(powder) and put in an oil bath set at 100 °C (Corning®, model PC-420D). The suspension was magnetically stirred at 300 rpm for a defined time interval (Table 1), and then the flask was removed from the oil bath. The suspension was left to cool for at least 30 min, and then transferred to a Büchner glass funnel (porosity 1) for purification. The solid was rinsed under vacuum with 95% ethanol (50 mL), distilled water (100 mL), 0.01 mol L^{-1} aqueous NaOH solution (100 mL), distilled water (100 mL), 0.01 mol L^{-1} aqueous HCl solution (100 mL), distilled water (100 mL), absolute ethanol (50 mL), and acetone (50 mL). Finally, the SBSPh was transferred to a Petri dish and dried in an oven at 85 °C for 90 min. The SBSPh was cooled in a desiccator until its weight was constant.

2.4. Design of experiments and statistical analysis

A 2^3 experimental design was created with eleven trials and triplicate at the center point to evaluate the best SBSPh adsorbent material synthesized for use in the removal of Co^{2+} and Ni^{2+} from single aqueous solutions. Three independent variables were evaluated: time (*t*, min), temperature (*T*, °C), and mole fraction of succinic anhydride (χ_{SA}).

The dependent variables (*DVs*) evaluated were weight gain (*wg*, %), total number of free carboxylic acid groups ($n_{T,COOH}$, mmol g^{-1}), and adsorption capacity for Co^{2+} and Ni^{2+} ($q_{Co^{2+}}$, mmol g^{-1}, $q_{Ni^{2+}}$, mmol g^{-1}).

A 2^2 experimental design was created with four trials and triplicate at the center point to evaluate the best experimental conditions for desorption and re-adsorption of metal ions. Two independent variables were evaluated: concentration of aqueous nitric acid

solution (C_{HNO_3}, mol L^{-1}) and desorption time (t, min). The *DVs* evaluated were desorption efficiency (E_{des}, %) and re-adsorption efficiency ($E_{re\text{-}ads}$, %).

The matrices of the experimental design were created using the Statistica 12.0 (StatSoft, Inc.), which was also used to evaluate the experimental results with routines for analysis of variance (ANOVA), standardized effects (Pareto's chart), and graphical analysis. Pure error was chosen for statistical significance and computation of standard errors, and the most complex model was used for both experimental designs. Statistical analyses were performed with a 95% significance level. An independent variable was considered as statistically significant for the evaluated response when the p-value was lower than 0.05 ($p < 0.05$).

2.5. Characterization of SBSPh

2.5.1. Weight gain and number of carboxylic acid groups

The weight gain (*wg*) after esterification of the hydroxyl groups of SB with succinic and phthalic anhydrides was determined gravimetrically. The total number of free carboxylic acid groups ($n_{T,COOH}$) released after esterification was determined by acid-base back-titration: 100.0 mg of SBSPh was weighed accurately into three 250 mL Erlenmeyer flasks, and 100.0 mL of a standardized aqueous 0.01 mol L^{-1} NaOH solution was added to these flasks. After the flasks had been mechanically stirred at 130 rpm for 1 h at 25 °C, the liquid and solid phases were separated by a single filtration (JP-41 filter paper) and three 20.0 mL aliquots of each liquid phase were titrated with a standardized aqueous 0.01 mol L^{-1} HCl solution until the endpoint of phenolphthalein. The value of $n_{T,COOH}$ was calculated using Eq. (1) [8]:

$$n_{\mathrm{T,COOH}} / \left(\mathrm{mmol\ g^{-1}}\right) = \left[\frac{C_{\mathrm{NaOH}} V_{\mathrm{NaOH}} - f\left(C_{\mathrm{HCl}} V_{\mathrm{HCl}}\right)}{w_{\mathrm{SBSPh}}} \right] \quad (1)$$

where C_{NaOH} and C_{HCl} (mmol L^{-1}) are the concentrations of the standardized NaOH and HCl solutions, respectively, V_{NaOH} (L) is the volume of the standardized NaOH solution, V_{HCl} (L) is the volume of the standardized HCl solution consumed in the titration, w_{SBSPh} (g) is the weight of SBSPh adsorbent, and f is a conversion factor (f = 100/20).

2.5.2. Point of zero charge (PZC)

To determine the PZC, 20.0 mL of aqueous 0.01 mol L^{-1} $NaNO_3$ solution (pH 3, 6 or 11, adjusted with aqueous 0.1 mol L^{-1} HNO_3 or 0.1 mol L^{-1} NaOH solutions) was added to 125 mL Erlenmeyer flasks containing different amounts of SBSPh adsorbent (0.01, 0.02, 0.1, 0.2, and 0.4 g) [15]. After the flasks had been mechanically stirred (Tecnal, model TE-424) at 130 rpm for 24 h at 25 °C, the equilibrium pH was measured (Hanna Instruments, model HI 223). Three curves of equilibrium pH against weight percentage of SBSPh were obtained and PZC was determined as the convergence point of these curves.

2.5.3. Specific surface area and pore size distribution

The specific surface area and pore size distribution of the SBSPh adsorbent were measured on a Quantachrome surface area and pore analyzer, model NOVA1200e®, by N_2 adsorption and desorption isotherms at 77.35 K. SBSPh was first degassed at 25 °C for 24 h under vacuum at 0.016 mmHg. Specific surface area was calculated using the method of Brunauer, Emmett and Teller (BET) [16] and the pore size distributions were calculated using the method of Barrett, Joyner and Halenda (BJH) [17].

2.5.4. Elemental analysis

The percentages of carbon, hydrogen, and nitrogen in SB and SBSPh samples were determined on a Perkin Elmer Series II CHNS/O 2400 analyzer (Shelton, USA). The samples were first dried in an oven at 85 °C for 1 h and analyzed in duplicate.

2.5.5. Fourier transform infrared (FTIR) spectroscopy

The IR spectra were recorded in an ABB Bomen MB 3000 FTIR spectrometer (Quebec, Canada) equipped with ZnSe optics and a deuterated triglycine sulfate detector set at a resolution of 4 cm^{-1} from 500 to 4000 cm^{-1} with 32 scans per sample. Samples of 1.0 mg were mixed with 100.0 mg of spectroscopy grade KBr and pressed in a hydraulic press at 6 tons for 0.5 min to prepare 13 mm KBr pellets (Pike CrushIR, model 181-1110, Pike Technologies, Canada). All samples were dried in an oven at 85 °C for 1 h before analysis.

2.5.6. ^{13}C Multi-CP solid-state nuclear magnetic resonance (^{13}C Multi-CP SS NMR)

^{13}C Multi-CP SS NMR experiments were performed on a Bruker Avance 400 NMR spectrometer, equipped with a Bruker 4-mm MAS double-resonance probe, at ^{13}C and ^{1}H frequencies of 100.5 and 400.0 MHz, respectively. The spinning frequency at 14 kHz was controlled by a pneumatic system that ensured a rotation stability higher than ~1 Hz. Typical $\pi/2$ pulse lengths of 4 and 3.5 µs were applied for ^{13}C and ^{1}H, respectively. Proton decoupling field strength of $\gamma B_1/2\pi$ = 100 kHz was used. ^{13}C quantitative spectra were measured by using the Multi-CP excitation method described by Johnson and Schmidt-Rohr [18]. A total of nine cross-polarization blocks were

implemented with 1 ms and RF amplitude increment (90–100%), while the cross-polarization before acquisition was executed with 0.8 ms and the same amplitude increment. The recycle delay was 2 s and the duration of the repolarization period t_z was 0.9 s [19].

Unlike the often-used CP-MAS, Multi-CP provides a homogeneous excitation of all chemical groups [18]. This allows estimation of the number of succinyl and phthalyl units adhered to the SBSPh structure. Regions 1 and 2 (Figure 3) are of interest for the calculation because the signals between 121 and 163 ppm are related to the aromatic rings, while the signals between 24 and 37 ppm are related to the ethylene groups of the succinyl group. Evaluation of the number of anhydrides introduced by chemical modification of SB was obtained by normalizing all the spectra relative to the area of the respective signal of cellulose carbon C-1, and then subtracting the spectra of raw SB from that of SBSPh. For each region of interest, the resulting area of this difference is proportional to number of carbons inserted in it relative to the number of C-1 carbons, i.e., by repetitive unity of cellulose (cellobiose dimer). Because there are six carbons per aromatic unit and two C-1 carbons per cellobiose unit, the intensity in region 1 was divided by three to obtain the percentage of aromatic rings introduced by the chemical modification. Similarly, the number of ethylene groups adhered was obtained directly by the C-1 normalized difference in region 2, because there are two ethylene groups in each succinyl group per repetitive unit of cellulose.

The crystallinity index (CI) was obtained using solid-state NMR by the areas of the peaks at 84 and 88 ppm, assigned to the C-4 carbon of amorphous (surface) and crystalline (internal) cellulose, respectively, as described in the literature [20, 21].

2.5.6.1.NMR relaxometry

NMR CPMG experiments were performed using a Bruker Minispec MQ-20 spectrometer operating with a magnetic field of 0.5 T (^{1}H Larmor frequency of 20 MHz). 50,000 echoes were acquired with echo times of 70 μs and recycle delays of 15 s. The CPMG decay curves were processed to obtain the T_2 distribution using a non-negative least square procedure also known as numerical Inverse Laplace Transform (ILT) [22, 23]. The obtained T_2 distributions were deconvoluted using log-gaussian functions to assess the contribution of each component in the pore structure. All measurements were performed in duplicate, and the ILT was performed on the CPMG decay given by the average of these two measurements.

To assess the pore structure of the materials, *N*,*N*-dimethylacetamide (DMAc, HPLC grade) was used as a molecular probe. In NMR relaxometry experiments, water is the most commonly used molecular probe for pore structure. However, it has been shown that in soft porous systems such as biomasses water alters the pore distributions. Because the interaction of DMAc with the cell wall is weaker, the use of this molecule does not significantly change the pore structures [24]. The samples were dried in a vacuum oven at 510 mmHg and 80 °C for 24 h. Then, they were saturated with DMAc and kept at a 570 mmHg vacuum overnight to fill the sample pores. The excess DMAc was removed through centrifuge filtration (Corning® Costar® Spin-X, 0.45 μm, nylon membrane), with a rotation frequency of 200 G for 1 min for all samples.

For fluids confined in nano- and micropores there is a close relation between the transverse relaxation time, T_2, and the surface-to-volume ratio of pores [25, 26]:

$$\frac{1}{T_2} = \left(\frac{1}{T_2}\right)_{\text{bulk}} + \rho\left(\frac{S}{V}\right) + \frac{D\left(\gamma G t_{\text{E}}\right)^2}{12} \qquad (2)$$

where ρ is the surface relaxivity constant, S and V are the pore surface and volume, respectively, D is the translational diffusion coefficient of the fluid, γ is the volume sink strength density, G is the magnetic field gradient associated to the field heterogeneity and t_E is the CPMG echo time. The last term in Eq. (2) shows that T_2 dependence on the translational diffusion is enhanced in a highly inhomogeneous magnetic field, but becomes unimportant for short t_E values, as used here. Thus, under these conditions and in the absence of fluid unbounded to pore surfaces, the relation between the T_2 relaxation rate and the pore size is given as follows:

$$\frac{1}{T_2} = \rho\left(\frac{S}{V}\right) = \frac{2\rho}{r} \tag{3}$$

where r is the characteristic size parameter [25]. The surface relaxivity constant depends on the particular porous media and is usually unknown. Thus, it is hard to obtain the actual pore sizes, or interstitial scales in this case, but the trends of T_2 indicate variations in the sizes of regions filled with the fluid. Larger T_2 values correspond to larger pores [27]. In a realistic scenario, the presence of a distribution of pore sizes and variations in the mobility of water molecules within the pores enable the CPMG decay, $S_{CPMG}(t)$, to be described as a weighted sum over single exponentials, as shown in Eq. (4):

$$S_{\mathrm{CPMG}}(t) = \int g(T_2) e^{-t/T_2} dT_2 \tag{4}$$

where $g(T_2)$ represents the transverse relaxation time distribution. $g(T_2)$ is determined from CPMG decay curves using the ILT procedure [22, 23].

2.5.7. Energy dispersive X-ray (EDX) spectroscopy

EDX images were recorded on a scanning electron microscope (JEOL, model 6510) coupled to an EDX spectrometer (Oxford, model X-Max) equipped with a tungsten filament at a voltage of 10 to 20 keV. Samples were first dried in an oven at 85 °C for 1 h before analysis. For EDX analysis, about 100 mg of sample was pressed in a hydraulic press (Pike, model 181-1110) with 6 tons for 1 min to obtain 13 mm pellets. All samples were sputter-coated with carbon in a modular high-vacuum coater (JEOL, model JEE-420).

2.6. Batch adsorption experiments

Adsorption of Co^{2+} and Ni^{2+} from single aqueous solutions was studied as a function of pH, contact time (kinetics), and initial metal ion concentration (isotherm). The typical procedure used in these studies was as follows: 100.0 mL of an aqueous metal ion (Co^{2+} or Ni^{2+}) solution at a known concentration prepared in buffer was transferred to a 250 mL Erlenmeyer flask and held at 25 °C in an orbital shaker incubator (Marconi, model MA-830) for 1 h. Then, 50 mg of SBSPh was weighed into cylindrical glass bottles (1.8 mm height × 2.2 mm diameter), added to the flask and stirred for a defined time interval. After this period, the liquid and solid fractions were separated by a single filtration (JP-41 filter paper) and the concentration of metal ion in the liquid phase was determined by flame atomic absorption spectrophotometer (Varian, model SpectrAA 50 B) at wavelengths of 240.7 nm and 232 nm for Co^{2+} and Ni^{2+}, respectively. The adsorption capacity (q) of the SBSPh adsorbent for Co^{2+} and Ni^{2+} was calculated using Eq. (5):

$$q_x \,/\, (\text{mmol g}^{-1}) = \frac{\left(C_{i,M^{2+}} - C_{x,M^{2+}}\right)V}{w_{SBSPh}} \qquad (5)$$

where q_x (mmol g^{-1}) is the adsorption capacity at time t ($x = t$) or equilibrium ($x = e$), V (L) is the volume of the metal ion solution, $C_{i,M^{2+}}$ and $C_{x,M^{2+}}$ (mmol L^{-1}) are the metal ion solution concentrations initially and at time t ($x = t$) or equilibrium ($x = e$), respectively, and w_{SBSPh} (g) is the weight of SBSPh.

The effect of pH on the adsorption process was evaluated over a pH range of 2.0 to 5.75, for an initial metal ion concentration of 0.850 mmol L^{-1} and 130 rpm at 25 °C. Kinetic and equilibrium studies were carried out at pH 5.75 and 130 rpm at 25 °C. The initial metal ion concentration used in kinetic studies was 0.850 mmol L^{-1} and contact times varied from 2 to 900 min for Co^{2+} and from 2 to 780 min for Ni^{2+}. Equilibrium studies were performed by varying the initial metal ion concentration over a range of 0.030 to 2.972 mmol L^{-1} for Co^{2+} and 0.032 to 3.223 mmol L^{-1} for Ni^{2+}. The contact time used in the equilibrium studies was 3 h for Co^{2+} and 2 h for Ni^{2+}. The experiments were carried out in duplicate and the results were averaged.

2.7. Desorption and reuse of the SBSPh adsorbent

SBSPh samples were loaded with Co^{2+} or Ni^{2+} using the procedure described in Section 2.6 with the following experimental conditions: initial metal ion concentration of 0.850 mmol L^{-1}, equilibrium time of 3 h for Co^{2+} and 2 h for Ni^{2+}, and pH of 5.75. 50 mg of SBSPh loaded with metal ions, oven-dried at 80 °C for 4 h, was weighed in cylindrical glasses, added to 125 mL Erlenmeyer flasks containing 50.0 mL of aqueous nitric acid solution, and stirred at 130 rpm at 25 °C in an orbital shaker (Tecnal, model TE-424, Piracicaba, São Paulo, Brazil) for different contact times. Then, the liquid and solid phases were separated and the concentration of metal ion in the liquid phase was determined as described in Section 2.6. The desorption efficiency (E_{des}, %) was calculated using Eq. (6) [28]:

$$E_{\text{des}} / \% = \left(\frac{C_{\text{e,M}^{2+}} V_{\text{HNO}_3}}{Q_{\text{T,max}} w'_{\text{SBSPh}}} \right) \times 100 \quad (6)$$

where $C_{\text{e,M}^{2+}}$ (mg L^{-1}) is the equilibrium metal ion concentration in the desorption solution, V_{HNO_3} (L) is the volume of the desorption solution, $Q_{\text{T,max}}$ (mg g^{-1}) is the maximum adsorption capacity of metal ion determined for SBSPh, w'_{SBSPh} (g) is the weight of the SBSPh in $w_{\text{SBSPh,M}^{2+}}$, which is the weight of the SBSPh loaded with metal ion. The value of w'_{SBSPh} is calculated using Eq. (7) [28]:

$$w'_{\text{SBSPh}} / g = \frac{w_{\text{SBSPh,M}^{2+}}}{\left[\left(\frac{Q_{\text{T,max}}}{1000} \right) + 1 \right]} \quad (7)$$

For experiments of reuse (re-adsorption) of the SBSPh adsorbent after desorption, samples of 50 mg of SBSPh loaded with metal ion recovered after desorption, dried in an oven at 85 °C for 2 h, were weighed in cylindrical glasses and added to 250 mL Erlenmeyer flasks containing 100.0 mL aqueous metal ion (0.850 mmol L^{-1}) solution. Further procedures used were described in Section 2.6.

For a single adsorption-desorption-re-adsorption cycle, the re-adsorption efficiency ($E_{\text{re-ads}}$, %) is calculated using Eq. (8) [28]:

$$E_{\text{re-ads}} / \% = \left(\frac{Q_{\text{re-ads,max}}}{Q_{\text{T,max}}} \right) \times 100 \quad (8)$$

where $Q_{\text{re-ads,max}}$ and $Q_{\text{T,max}}$ (mg g^{-1}) are the maximum adsorption capacities determined in the re-adsorption and adsorption of metal ions on the SBSPh adsorbent, respectively. The value of $Q_{\text{re-ads,max}}$ is calculated using Eq. (9) [28]:

$$Q_{\text{re-ads,max}} / \left(\text{mg g}^{-1}\right) = \frac{\left[\left(w_{\text{SBSPh,M}^{2+}} - w'_{\text{SBSPh}}\right)\left(1 - E_{\text{des}}/100\right)\right] - \left[\left(C_{\text{i,M}^{2+}} - C_{\text{e,M}^{2+}}\right)V_{\text{M}^{2+}}\right]}{w'_{\text{SBSPh}}} \quad (9)$$

2.8. Isothermal titration calorimetry (ITC)

Calorimetry studies of adsorption were carried out in an isothermal titration nanocalorimeter (TA Instruments, model TAM III) equipped with two 4 mL calorimetric cells (sample cell and reference cell) and controlled by the TAM assitant™ software. For the experiments, 5.60 mg of SBSPh was weighed into the sample cell, and then both cells were filled with 2.7 mL of acetic acid/sodium acetate buffer at pH 5.75. After the system achieved thermal equilibrium, a concentrated aqueous solution of metal ion (200.0 mg Co^{2+} L^{-1} or 200.6 mg Ni^{2+} L^{-1}), prepared in the same solvent, was titrated step-by-step the suspension into the sample cell. Injections of 15 μL metal ion solution were performed consecutively using a 500 μL Hamilton syringe controlled by a piston pump, and the time interval between two consecutive injections was 35 min. The suspension in the sample cell was stirred at 180 rpm using a helix stirrer. In order to discount the adsorbate dilution energy, similar experiments were performed without the presence of the adsorbent in the sample cell. Prior to each experiment the samples were degassed for 10 min. The experiments were performed in duplicate at 25.0000 ± 0.0001 °C. The adsorption enthalpy change ($\Delta_{\text{ads}}H$) was calculated by Eq. (10):

$$\Delta_{\text{ads}}H = \frac{\sum_{i=1}^{m}\left(q_{\text{i,int}} - q_{\text{i,dil}}\right)}{\sum_{i=1}^{m} n_{\text{i}}} \quad (10)$$

where $q_{\text{i,int}}$ and $q_{\text{i,dil}}$ are the absorbed or released heat in the sample cell after each injection i for the titration experiments performed in the presence and absence of the

adsorbent, respectively, and n_i is the amount of metal ion, in mol, that was adsorbed onto the SBSPh in the same injection.

3. Modeling the experimental data

3.1. Kinetic data

Four kinetic models were used to model the adsorption of Co^{2+} and Ni^{2+} onto the SBSPh adsorbent: pseudo-first (PFO) and pseudo-second-order (PSO), Boyd, and intraparticle diffusion (IPD) [8, 29].

The PFO model [30] is shown in Eq. (11):

$$q_t \,/\,(\text{mmol g}^{-1}) = q_e\left[1-\exp\left(-k_1 t\right)\right] \tag{11}$$

where k_1 (min^{-1}) is the PFO rate constant.

The PSO model [31] is shown in Eq. (12):

$$q_t \,/\,(\text{mmol g}^{-1}) = \frac{k_2 q_e^2 t}{1+k_2 q_e t} \tag{12}$$

where k_2 ($\text{g mmol}^{-1}\ \text{min}^{-1}$) is the PSO rate constant.

The IPD model [32] is shown in Eq. (13):

$$q_t \,/\,(\text{mmol g}^{-1}) = k_i t^{1/2} + C \tag{13}$$

where k_i ($\text{mmol g}^{-1}\ \text{min}^{-1/2}$) is the IPD rate constant and C (mmol g^{-1}) is the intercept, which is a constant that may be related to the boundary layer thickness.

The model of Boyd [33] is shown in Eq. (14):

$$f = 1 - \frac{6}{\pi^2}\sum_{n=1}^{\infty}\frac{1}{n^2}\exp\left(-n^2 Bt\right) \quad (14)$$

where f is the fractional coverage ($f = q_t\, q_e^{-1}$) at different times t and Bt is a function of f. Solutions for Eq. (14) were provided by Reichenberg [34] using Fourier transform and are given by Eqs. (15) and (16). For $f > 0.85$, Eq. (15) was used, while for $f < 0.85$, Eq. (16) was used:

$$Bt = -0.4977 - \ln\left(1 - f\right) \quad (15)$$

$$Bt = \left(\sqrt{\pi} - \sqrt{\pi - \frac{\pi^2 f}{3}}\right)^2 \quad (16)$$

The effective diffusion coefficient D_i [29] was calculated using Eq. (17):

$$D_i \,/\left(\mathrm{m^2\ min^{-1}}\right) = \frac{Br^2}{\pi^2} \quad (17)$$

where r is the radius of the SBSPh particles, assuming a spherical shape ($r = 0.250 \times 10^{-3}$ m).

3.2. Equilibrium data

Equilibrium data were modeled by the Langmuir, Sips, Redlich–Peterson and Dubinin–Radushkevich isotherm models [8, 29].

The Langmuir model [35] is shown in Eq. (18):

$$q_e \,/\left(\mathrm{mmol\ g^{-1}}\right) = \frac{\mathrm{Q_{max}}\, b\mathrm{C_e}}{1 + b\mathrm{C_e}} \quad (18)$$

where Q_{max} (mmol g^{-1}) is the maximum adsorption capacity and b (L $mmol^{-1}$) is the Langmuir binding constant.

The Sips model [36] is shown in Eq. (19):

$$q_e / \left(\text{mmol g}^{-1}\right) = Q_{max} \frac{\left(bC_e\right)^{1/n}}{1+\left(bC_e\right)^{1/n}} \quad (19)$$

where n is a parameter that characterizes the heterogeneity of the adsorption system.

The Redlich–Peterson (R–P) model [37] is shown in Eq. (20):

$$q_e / \left(\text{mmol g}^{-1}\right) = \left(\frac{K_R C_e}{1+a_R C_e^{\beta}}\right) \quad (20)$$

where K_R (L g^{-1}) and a_R (L $mmol^{-1}$) are the R–P isotherm constants and β is the R–P isotherm exponent (dimensionless), assuming values between 0 and 1.

The Dubinin–Radushkevich (D–R) model [38] is shown in Eq. (21):

$$q_e / \left(\text{mmol g}^{-1}\right) = q_s \exp\left(-B\varepsilon^2\right) \quad (21)$$

where q_s (mmol g^{-1}) is the maximum adsorption capacity, B (mol^2 kJ^{-2}) is the solid characteristic energy toward a reference adsorbate (originally defined as benzene), and ε is the Polanyi's potential, which is given by Eq. (22):

$$\varepsilon = RT \ln\left(1+\frac{1}{C_e}\right) \quad (22)$$

where R is the gas constant (8.314 J K^{-1} mol^{-1}) and T (K) is the absolute temperature.

The characteristic energy of adsorption, E, can be estimated using Eq. (23):

$$E / \left(\text{kJ mol}^{-1}\right) = \frac{1}{\sqrt{2B}} \tag{23}$$

3.3. Approach for calculation of thermodynamic parameters of adsorption

The variation of the standard free energy of adsorption ($\Delta_{ads}G°$) was calculated using Eq. (24):

$$\Delta_{ads}G^{\circ} = -RT \ln K_a \tag{24}$$

where K_a (dimensionless) is the thermodynamic equilibrium constant, which was calculated as the ratio between the Langmuir constant (b) and the activity coefficient of the metal ion in solution at equilibrium (γ_e), as shown in Eq. (25) [39]:

$$K_a = \frac{b}{\gamma_e}\left(1 \text{ mol L}^{-1}\right) \tag{25}$$

According to the Debye–Hückel extended limit law, γ_e is a function of the ionic strength (I_e) of the solution, as shown in Eq. (26):

$$\log \gamma_e = \frac{-0.51 z^2 \sqrt{I_e}}{1 + \left(\frac{\alpha \sqrt{I_e}}{305}\right)} \tag{26}$$

where z is the charge on the metal ion, I_e (mol L^{-1}) is the ionic strength of the solution at equilibrium, and α is the size of the hydrated metal ion (α = 600 pm for Co^{2+} and Ni^{2+}) [8].

In order to obtain the variation of the standard enthalpy of adsorption ($\Delta_{ads}H°$), the $\Delta_{ads}H$ values obtained by ITC were plotted against the equilibrium concentration of metal ion in the sample cell (C_e), and $\Delta_{ads}H°$ was determined by extrapolating the curve

of $\Delta_{ads}H$ against C_e to C_e equals zero. The variation of the standard entropy of adsorption ($\Delta_{ads}S°$) was determined from the classical thermodynamic relationship, as shown in Eq. (27):

$$\Delta_{ads}G^{\circ} = \Delta_{ads}H^{\circ} - T\Delta_{ads}S^{\circ} \quad (27)$$

4. Results and discussion

4.1. Characterization of sugarcane bagasse

The chemical composition (wt %) of solvent-extracted SB used to prepare the SBSPh adsorbent was 45.48 ± 0.31 cellulose, 30.55 ± 0.54 hemicelluloses, and 23.78 ± 0.76 lignin. This chemical composition was in good agreement with those reported by Gurgel et al. [40] and Baêta et al. [13].

4.2. Evaluation of synthesis and application of SBSPh adsorbent for adsorption of Co^{2+} and Ni^{2+}

The evaluation of different reaction conditions for synthesizing SB cellulose mixed ester using the classic trial-and-error method can be considered extremely time-consuming and costly. Furthermore, it does not include the interaction effects among the synthesis parameters [41]. To overcome this problem, different synthesis conditions were evaluated by a 2^3 experimental design, aiming to understand better how changes in the synthesis parameters such as T, t and χ_{SA} affect the important response variables such as wg, $n_{T,COOH}$, $q_{Co^{2+}}$ and $q_{Ni^{2+}}$, allowing improvements of the environmental applications of the synthesized material.

Pareto's charts of standardized effects for the responses $q_{Co^{2+}}$ and $q_{Ni^{2+}}$ are shown in Supplementary Figure 1. Table 1 shows the 2^3 experimental design used to evaluate the

effect of the synthesis parameters T, t and χ_{SA} on the responses wg, $n_{T,COOH}$, $q_{Co^{2+}}$ and $q_{Ni^{2+}}$. The independent variables T (8.446) and t (20.384) had significant positive effects on $q_{Ni^{2+}}$, while the independent variable χ_{SA} (–5.017) had a significant negative effect on $q_{Ni^{2+}}$ (Table 1). This means that higher levels of T and t yielded higher values of $q_{Ni^{2+}}$, while lower levels of χ_{SA} yielded higher values of $q_{Ni^{2+}}$. In contrast, no independent variable was significant for response $q_{Co^{2+}}$. However, the negative effect of χ_{SA} (–5.017) on $q_{Ni^{2+}}$ was higher than the negative effect of χ_{SA} (–3.405) on $q_{Co^{2+}}$, indicating that the χ_{SA} affected more the value of q for Ni^{2+} than that for Co^{2+} for the synthesized material. This also suggested that PA was a better ligand for chelating both metal ions than was SA. The first-degree polynomial equation used to model the response $q_{Ni^{2+}}$ presented lack of fit (LOF) (p = 0.0226), indicating that this response cannot be modeled by a linear model. However, the response $q_{Co^{2+}}$ did not present LOF (p = 0.0715). Thus, more experimental data would be required for optimization and modeling the synthesis of SB cellulose mixed ester by means of a quadratic model (2^3 central composite design, for example). However, as the aim of this study was to evaluate the effect of different synthesis conditions on the values of $q_{Co^{2+}}$ and $q_{Ni^{2+}}$, within the range of values evaluated for independent variables T, t and χ_{SA}, the best responses ($q_{Co^{2+}}$ and $q_{Ni^{2+}}$) were obtained at the experimental condition 4 (T = 100 °C, t = 660 min, χ_{SA} = 0.2). Thus, this experimental condition was chosen to be reproduced in a larger scale (15-fold increase in the amount of reactants) for the subsequent adsorption studies.

4.3. Characterization of SBSPh adsorbent

4.3.1. Weight gain, number of carboxylic acid groups, elemental analysis, specific surface area and pore size distribution

The SBSPh material synthesized on a larger scale using experimental condition 4 was obtained with a *wg* of 60.52% and a $n_{T,COOH}$ of 3.51 mmol g^{-1}, which were in good agreement with the values of *wg* and $n_{T,COOH}$ for SBSPh synthesized on the smaller scale (Table 1). The contents of carbon, hydrogen and nitrogen in SB and SBSPh were 44.93(± 1.07)% and 53.42(± 0.47)%, 6.07(± 0.12)% and 4.98(± 0.01)%, and 0.26(± 0.06)% and 1.30(± 0.00)%, respectively, showing an increase in carbon content and a decrease in hydrogen content in comparison to raw SB. Since PA (C = 64.43% and H = 3.38%) and SA (C =53.00% and H = 4.99%) have a higher carbon content and a lower hydrogen content than SB, these results suggested that the chemical modification of SB with both SA and PA was successful. The small nitrogen content in SB and SBSPh was due to the presence of proteins that were not totally removed by Soxhlet extraction of SB, and the presence of residual solvent (Py) that was not totally removed in the purification of SBSPh. The SBSPh adsorbent had a specific surface area of 5.4 m^2 g^{-1}, an average and a maximum pore diameter size of 35.9 Å and 566.5 Å, respectively, and a total pore volume of 5.8×10^{-3} cm^3 g^{-1}.

4.3.2. FTIR spectroscopy

Figure 2a shows the FTIR spectra of SB and SBSPh. The main changes noticed in the IR spectrum of SBSPh in comparison to that of SB were: (*i*) a widening of the band at 3425 cm^{-1} related to the intramolecular hydrogen bonding between the hydrogen of carboxylic acid group and the oxygen of the ester carbonyl group; (*ii*) the appearance of two bands at 2653 and 2511 cm^{-1} related to the stretching of hydrogen bonding of carboxylic acid dimers; (*iii*) a strong band at 1731 cm^{-1} related to stretching of unconjugated (1743 cm^{-1}) [42] and conjugated (1724 cm^{-1}) [11] carbonyl ester groups from succinyl and phthalyl moieties, respectively, which appeared overlapped; (*iv*) the appearance of a band at 1490 cm^{-1} related to the stretching of C=C bonds of the

phthalate moiety, which is shifted to the right in comparison to the stretching of C=C (1500 cm^{-1}) bonds of SB lignin; (*v*) a band at 1282 cm^{-1} related to the stretching of the C–O of ester and carboxylic acid groups; and (*vi*) a band at 748 cm^{-1} related to C–H out-of-plane bending of the 1,2-disubstituted aromatic ring of the phthalate moiety [43].

Figure 2b shows the FTIR spectra of SBSPh and SBSPh loaded with Co^{2+} (SBSPh-Co) and Ni^{2+} (SBSPh-Ni). The major change noticed in the IR spectrum of SBSPh in comparison to those of SBSPh-Co and SBSPh-Ni was the appearance of a band at 1685 cm^{-1} related to the stretching of carboxylate carbonyl group, which was split into two new bands at 1589 and 1557 cm^{-1} related to the symmetrical and asymmetrical stretching of carboxylate groups complexed with the metal ion [44]. These IR bands suggested that there was no appreciable difference between the complexes formed by Co^{2+} and Ni^{2+}, which will be confirmed by the small difference between the changes of adsorption enthalpy of both metal ions (Section 4.6). Furthermore, the IR bands related to hydrogen bonding of carboxylic acid dimers (2653 and 2511 cm^{-1}) disappeared in the spectra of SBSPh-Co and SBSPh-Ni in comparison to that of SBSPh. The splitting of the band related to the carboxylate group complexed with metal ion was also observed by Łyszczek [44] and suggested that the carboxylate groups are not equivalent, which is in good agreement with the chemical structure of SBSPh. In addition, the presence of carboxylate groups involved in the adsorption of Co^{2+} and Ni^{2+} indicated that adsorption of both metal ions involved a contribution from electrostatic attraction.

4.3.3. ^{13}C Multi-CP solid-state nuclear magnetic resonance spectroscopy, relaxometry and crystalline index

Figure 3 shows ^{13}C Multi-CP SS NMR spectra of SB and SBSPh. The ^{13}C NMR spectrum of raw SB is similar to those reported by Chandel et al. [45], Bernardinelli et

al. [19], Liu et al. [46], Rezende et al. [47], and Wang et al. [48]. Seventeen signals were identified in the ^{13}C NMR spectrum of SB for carbons of cellulose, hemicelluloses and lignin. Signal 10 (105.3 ppm) is related to the carbon at C-1 of the β-D-anhydroglucose unity (AGU) of cellulose. Signals 7 (84.1 ppm) and 8 (88.6 ppm) are related to the carbon at C-4 while the signals 5 (72.6 ppm) and 6 (74.8 ppm) are related to the carbons at C-2, C-3 and C-5 of AGU. Signals 3 (62.5 ppm) and 4 (64.6 ppm) are related to the carbon at C-6 [49, 50] of AGU. The signals related to the lignin are mainly in the range of 110 to 160 ppm and are relatively wider due to the complexity of the structure of this macromolecule. Signal 2 (55.7 ppm) is related to the carbon of the methoxyl groups (–O–CH_3) of aromatic moieties present in lignin structure. Signals 1 (21.1 ppm), 9 (99.5 ppm), 16 (168.8 ppm), and 17 (172.8 ppm) are related to the carbons of hemicelluloses, with the latter signals being related to the carbons of carboxyl groups. The chemical shifts of SB and SBSPh are similar, but there are some differences, indicated by two regions assigned in Figure 3 as region 1 and region 2. In region 1, which is comprised of the signals between 120 and 140 ppm, a single wide signal appeared in the SBSPh spectrum that is related to the signal of aromatic carbons of the phthalyl molecule introduced into SB, in addition to the aromatic units present in lignin. Region 2 is comprised of signals between 24 and 40 ppm. No signal was observed in the SB spectrum this region, but in the SBSPh spectrum there is a low-intensity signal related to ethylene carbons (–CH_2–CH_2–) of the succinyl molecule. Similar signals were reported by Melo et al. [49] and Melo et al. [50] for cellulose modified with succinic anhydride and phthalic anhydride, respectively. The significant increase in the signals 16 and 17 indicated an increase in the number of carboxylic acid groups in the structure of SBSPh.

The quantification of ^{13}C NMR spectrum of SBSPh revealed that for each cellobiose unit there are 0.4 ± 0.02 phthalyl units and 0.33 ± 0.02 succinyl units chemically bonded to SBSPh adsorbent material, i.e., a total of 0.73 SA and PA units were introduced by each cellobiose unit. Figure 4 illustrates the structure of SBSPh. This result confirms that SB cellulose succinate phthalate was successful synthesized by a simple one-pot synthesis method, contributing to the literature with a low-cost method for the preparation of different materials for technological applications.

The CI showed no variation between the two samples, with values of 0.21 ± 0.02 for SB and 0.22 ± 0.02 for SBSPh. This indicates that the introduction of SA and PA does not change the microstructure of the cellulose, keeping unaltered the ratio between surface (amorphous) and bulk (crystalline) cellulose.

Figure 5 shows the T_2 distributions obtained from the ILTs for each sample. There are three components related to different hierarchical structures of the lignocellulosic structure of SB. The first are the interstitial spaces on the surface of cellulose microfibrils (inner microfibrils) [23], with T_2 values of a few milliseconds and associated with a pore radius of a few nanometers. The spaces between the cellulose microfibrils (cell wall) [51] are related to T_2 values between 10^{-2} and 10^{-1} s and pore radius of a few dozen nanometers. The biggest interstitial scale measurable by NMR relaxometry is the lumens, with T_2 values ranging from 10^{-1} to 3 s and pore radius from 100 nm to a few µm. As shown in Table 2 the most prominent changes upon the chemical modification, compared with the pristine sample, is a decrease in the average inter-microfibril spaces (cell wall) and an enlargement of the lumen while the inner microfibril component remains unchanged. This is an indication that the aromatic rings and CH_2 groups are occupying spaces, which were previously free, mainly at the cell-wall scale. This suggests that the chemical modification takes place mostly on the

cellulose microfibril surface; this is also supported by the SS NMR results showing that the surface-to-bulk cellulose ratio is the same in both samples.

The amount of DMAc in each interstitial space, which is proportional to the volume of pores accessed by the fluid, can be measured by the relative area of its respective log-gaussian component in the T_2 distribution. Table 3 presents the relative areas for each deconvoluted component in the T_2 distributions. A smaller accessibility of DMAc in the cell wall was observed, which is another indication of the cell wall scale being the most affected by the insertion of the phthalyl and succinyl molecules, i.e., the chemical modification of cellulose occurs mostly on the microfibril surfaces.

4.4. Batch adsorption studies

4.4.1. Effect of solution pH on metal ion removal

Figure 6 shows the effect of solution pH on the values of q_e for Co^{2+} and Ni^{2+} adsorption on SBSPh. The values of q_e increased with increase in the solution pH from 2.0 to 5.75, indicating that electrostatic interactions took place in the adsorption process. In the pH range evaluated, the net surface charge of SBSPh depended on the solution pH. At pH lower than the PZC (2.69 ± 0.04), SBSPh had a positive net surface charge, which contributed to the removal of Co^{2+} and Ni^{2+} by electrostatic attraction. However, at pH values higher than PZC, the deprotonation of the carboxylic groups of succinate and phthalate moieties changed the net surface charge of SBSPh to negative, which contributed to attractive electrostatic interactions between the adsorbent and the metal ions. Therefore, there was an increase in the removal of the metal ions as solution pH increased. Over the pH range evaluated, the highest value of q_e for both metal ions was attained at pH 5.75, which was the maximum pH value investigated to avoid the

formation and consequent adsorption of hydrolyzed species such as $Co(OH)^+$ and $Ni(OH)^+$ ($Ksp_{Co(OH)_2} = 5.92 \times 10^{-15}$, $Ksp_{Ni(OH)_2} = 5.48 \times 10^{-16}$) [52].

4.4.2. Adsorption kinetics

Table 4 shows the kinetic parameters for adsorption of Co^{2+} and Ni^{2+} on SBSPh estimated from nonlinear (PFO and PSO) and linear (IPD and Boyd) regression analyses of the experimental data (Supplementary Table 1). Plots of q_t against t and kinetic curves fit to experimental data are shown in Supplementary Figure 2. The adsorption equilibria were attained in 180 and 120 min for Co^{2+} and Ni^{2+}, respectively, and were similar to those reported by Ramos et al. [11], who studied the adsorption of Co^{2+} (t_e = 180 min) and Ni^{2+} (t_e = 180 min) on SB modified with phthalic anhydride. For both metal ions, the PSO model described better the adsorption kinetics based on higher values of R^2 and R^2_{adj} and smaller value of χ^2_{red} in comparison to the PFO model. However, the PFO model estimated better the value of q_e for Ni^{2+} adsorption on the SBSPh adsorbent.

Supplementary Figures 3 and 4 show the experimental kinetic data fit with the IPD and Boyd kinetic models, respectively. The adsorption of Co^{2+} and Ni^{2+} on the SBSPh adsorbent exhibited three stages (Supplementary Figure 3); however, both straight lines adjusted to the first stages of Co^{2+} and Ni^{2+} adsorption did not intersect the origin ($C \neq 0$), suggesting that adsorption of Co^{2+} and Ni^{2+} on SBSPh was controlled by diffusion through the thin water film surrounding the SBSPh adsorbent particles, and probably changed to intraparticle diffusion until equilibrium was reached [8, 53]. Boyd's plots (Supplementary Figure 4) were linear in the initial adsorption time interval and did not intersect the origin; however, the values of the slopes of Boyd's plots (B) for Co^{2+} and Ni^{2+} adsorption were close to zero, indicating that external mass transfer through the

boundary layer surrounding the SBSPh adsorbent particles may be the rate-limiting step controlling the adsorption. In addition, the similar values of D_i for adsorption of both metal ions (Table 4) indicated that the diffusivities of Co^{2+} and Ni^{2+} through SBSPh particles were of the same order.

4.4.3. Adsorption isotherms

Table 5 shows the isotherm parameters for adsorption of Co^{2+} and Ni^{2+} on SBSPh estimated from nonlinear regression analysis of the experimental data (Supplementary Table 2) with the Langmuir, Sips, Redlich–Peterson and Dubinin–Radushkevich isotherm models. Adsorption isotherms and isotherms curves fit to experimental data are shown in Supplementary Figure 5. The adsorption isotherms for both metal ions exhibited isotherm type I profiles, where a plateau was observed, characterizing the saturation of the adsorbent surface sites. The Sips model described better the adsorption, based on higher values of R^2 and R^2_{adj} and smaller values of χ^2_{red} and *RSS* in comparison to the Langmuir model. However, the Sips model is a combination of the Langmuir and Freundlich [12] models, and is reduced to the Langmuir model when parameter *n* is equal to unity. The values of $n_{Co^{2+}}$ and $n_{Ni^{2+}}$ (Table 5) were closer to unity, which suggested the formation of a monolayer of metal ions on the SBSPh adsorbent surface [54]. Coordination numbers (*CN*) [42] of the SBSPh adsorbent for adsorption of Co^{2+} and Ni^{2+} were 7.7 and 7.5, respectively, suggesting that not all carboxylic acid groups introduced onto the SBSPh adsorbent were available to form an interaction with a metal ion. This probably led to a decrease in the adsorption capacity of the SBSPh adsorbent due to the aleatory modification of SB with two different carboxylic acid anhydrides in a one-pot reaction, in comparison to the SB modified with PA reported by Ramos et al. [11] (Table 8).

4.5. Energy dispersive X-ray (EDX) spectroscopy

EDX spectroscopy was used to map the surface of the SBPSh samples loaded with Co^{2+} and Ni^{2+} (SBSPh-Co^{2+} and SBSPh-Ni^{2+}) and to analyze the distribution of metal ions on the SBSPh surface. The micrographs recorded for SBSPh-Co^{2+} and SBSPh-Ni^{2+} are shown in Figure 6. These micrographs show that adsorbed metal ions were not distributed homogeneously over the surface of the SBSPh adsorbent, corroborating the hypothesis that not all carboxylic groups are involved in the adsorption of metal ions and that the carboxylic groups closer to each other are probably more available to adsorb metal ions and to form more stable complexes.

4.6. Isothermal titration calorimetry (ITC)

The ITC technique allows the determination of the amount of energy in the form of heat absorbed or released by a system when it has its composition changed by a titration process [55]. Here, ITC was used to determine the enthalpy change associated with the adsorption of Co^{2+} and Ni^{2+} on SBSPh. Figure 7 shows the adsorption enthalpy change ($\Delta_{ads}H$) of Co^{2+} and Ni^{2+} on the SBSPh adsorbent surface as a function of the amount of adsorbed metal ion at pH 5.75 and 25 °C. The $\Delta_{ads}H$ values were positive in the range of q_e evaluated, indicating that the adsorption process of Co^{2+} and Ni^{2+} on SBSPh is endothermic. For both metal ions and at low surface coverages, the $\Delta_{ads}H$ values did not change as q_e increased. For Ni^{2+} adsorption, from a value of q_e of 0.025 mmol g^{-1}, a slight increase of the $\Delta_{ads}H$ values could be observed when the q_e values increased, which was also observed for Co^{2+} adsorption; however, in a smaller proportion. This result, in addition to the similar $\Delta_{ads}H$ values calculated for the adsorption of both metal ions, suggested that the subprocess and the interactions involved in the adsorption of Co^{2+} and Ni^{2+} on SBSPh are the same.

The small variation in the $\Delta_{ads}H$ values may suggest, at first, that the adsorptive sites have similar energies, which would agree with the modeling of the adsorption isotherms, where the Sips model described better the Co^{2+} and Ni^{2+} adsorption. However, it is known that the adsorptive sites of the SBSPh adsorbent are heterogeneous in nature and that the adsorption mechanism is based on the electrostatic attraction between the negatively charged carboxylic groups ($R–COO^{-}$) and the positively charged metal ions (M^{2+}). Therefore, this result could suggest that the metal ions do not distinguish the carboxylate groups present in the succinate and phthalate moieties or there is an energy compensation from the different subprocess that governed the adsorption.

In order better to describe the adsorption phenomena of the metal ions on SBSPh, the $\Delta_{ads}H$ values were expressed as a sum of three terms associated with the contribution of three independent subprocesses that occurred simultaneously during adsorption, as shown in Eq. (28):

$$\Delta_{ads}H = \Delta_{desol}H^{\text{SBSPh sites-metal ion}} + \Delta_{int}H^{\text{SBSPh sites-metal ion}} + \Delta_{int}H^{\text{metal ion-metal ion}} \quad (28)$$

where $\Delta_{ads}H^{desol}$ is the enthalpy change associated with the desolvation of both metal ions and adsorbent surface sites (subprocess *i*), $\Delta_{ads}H^{\text{SBSPh sites-metal ion}}$ is the enthalpy change associated with the formation of interactions between the metal ions and adsorbent surface sites (subprocess *ii*), and $\Delta_{ads}H^{\text{metal ion-metal ion}}$ is the enthalpy change associated with the formation and disruption of metal ion–metal ion interactions on the adsorbent surface and in the bulk solution, respectively (subprocess *iii*).

The subprocesses *i* and *iii*, which occur with disruption and formation of intermolecular interactions, can be exothermic or endothermic, while the subprocess *ii* is always exothermic.

At the beginning of the adsorption process, when the surface coverage and the metal ion concentration in the bulk solution were low, the contribution of $\Delta_{ads}H^{\text{metal ion-metal ion}}$ for $\Delta_{ads}H$ could be disregarded, and Eq. (28) became $\Delta_{ads}H = \Delta_{ads}H^{\text{desol}} + \Delta_{ads}H^{\text{SBSPh-metal ion}}$. Therefore, positive values of $\Delta_{ads}H$ for the global process were observed because the subprocess *i* was endothermic and the values of $\Delta_{ads}H^{\text{desol}}$ were greater, in modulus, than the values of $\Delta_{ads}H^{\text{SBSPh-metal ion}}$. At higher surface coverages, the subprocess *iii* became important and contributed with the slight increase of the $\Delta_{ads}H$ values, which was mainly attributed to the repulsive metal ion–metal ion interactions on the SBSPh surface that made the term $\Delta_{ads}H^{\text{metal ion-metal ion}}$ positive. Probably, that effect was not more pronounced because the values of $\Delta_{ads}H^{\text{desol}}$ and $\Delta_{ads}H^{\text{SBSPh-metal ion}}$ depended on the concentration of metal ions in the solution and on the surface of the adsorbent, and the energies associated with all subprocesses could be compensating each other, and therefore generating values of $\Delta_{ads}H$ practically constant over the range of q_e investigated.

The results presented in this study are different in some aspects from those obtained by Xavier et al. [56], who studied the adsorption of the same metal ions on the surface of SB functionalized with trimellitic anhydride (STA). In particular, the $\Delta_{ads}H$ values for adsorption of Co^{2+} and Ni^{2+} on STA were less positive than those for adsorption of these metal ions on SBSPh. Moreover, contrary to the results obtained in the present study, where the values of $\Delta_{ads}H$ increased slightly with increased surface coverage, when the adsorption occurred on STA, the values of $\Delta_{ads}H$ decreased as q_e increased.

These results show that the thermodynamics of adsorption of metal ions can be modulated by the type of anhydride used to modify the SB.

4.7. Thermodynamic parameters of adsorption

Table 6 shows the thermodynamic parameters for adsorption of metal ions on the SBSPh adsorbent. The $\Delta_{ads}G°$ values were negative for both metal ions, indicating that they concentrate preferentially on the surface of the SBSPh at equilibrium under standard conditions. The $\Delta_{ads}H°$ values were positive, suggesting that the adsorption of both metal ions on the SBSPh adsorbent is endothermic. The magnitude of these values indicated a physisorption interaction between SBSPh adsorbent and metal ions. The term $T\Delta_{ads}S°$, associated to the entropic contribution, was also positive and had greater magnitude than the value of $\Delta_{ads}H°$ for adsorption of both metal ions, thereby indicating entropically driven adsorption processes. The entropy increase was attributed to the water molecules released from the solvation layer of metal ions and the SBSPh adsorption surface sites, which compensated the loss in the configurational entropy associated with the migration of metal ions from the bulk solution to the surface of the SBSPh adsorbent.

4.8. Multivariate evaluation of metal ions desorption from SBSPh adsorbent

Table 7 shows the 2^2 experimental design used to evaluate the effect of desorption parameters C_{HNO_3} and t on the response E_{des}.

Pareto's charts of standardized effects for response E_{des} for Co^{2+} and Ni^{2+} from SBSPh adsorbent are shown in Supplementary Figure 6. Both independent variables C_{HNO_3} (Co^{2+} = 17.934, Ni^{2+} = 20.037) and t (Co^{2+} = 39.043, Ni^{2+} = 20.037) had significant positive effects on E_{des}, while the interaction between them ($C_{HNO_3} \times t$) (Co^{2+} = –12.181,

Ni^{2+} = –14.312) had significant negative effects on E_{des}. This means that higher levels of C_{HNO_3} or t yielded higher values of E_{des} for both metal ions. In contrast, the interactions between variables C_{HNO_3} and t indicated that to obtain higher values of E_{des} for Co^{2+} and Ni^{2+}, one variable should be set at a higher level while the other variable should be set at a lower level. The first-degree polynomial equation used to fit the response E_{des} did not exhibited LOF for Ni^{2+} (p = 0.540), but had LOF for Co^{2+} (p = 0.030), suggesting that the experimental data obtained for $E_{des,Ni^{2+}}$ showed linear behavior, while those for $E_{des,Co^{2+}}$ did not show linear behavior. Thus, the mechanism for the desorption of Co^{2+} and Ni^{2+} from SBSPh adsorbent is suggested as ion exchange, because at pH 0.0 the concentration of H_3O^+ ions is sufficiently high to replace a metal ion, resulting in a protonated carboxylic group and releasing a metal ion from a SBSPh surface site to the bulk solution [8, 11].

Analyzing the data presented in Table 7, within the experimental data range evaluated the desorption condition performed at a C_{HNO_3} of 1.0 mol L^{-1} and a t of 45 min was the best condition obtained for desorption of both metal ions from the SBSPh adsorbent.

4.9. Reuse of the SBSPh adsorbent

All SBPSh adsorbents subjected to desorption were evaluated for re-adsorption of Co^{2+} and Ni^{2+} from single aqueous solutions, and the values of $E_{re\text{-}ads}$ are shown in Table 7. After desorption and re-adsorption of Co^{2+}, the SBSPh adsorbent exhibited a lower capacity to remove Co^{2+} from aqueous solution for almost all re-adsorption conditions evaluated, with the exception of condition 2. In contrast, after desorption and re-adsorption the SBSPh adsorbent exhibited an equal or higher capacity to remove Ni^{2+} from single aqueous solutions. These results showed that is possible to use SBPSh

adsorbent material in a wastewater treatment plant without significant losses in its adsorption capacity after an adsorption-desorption-re-adsorption cycle.

4.10. Comparison of SBSPh adsorbent with other adsorbent materials

Table 8 shows different adsorbent materials that have been applied for the removal of Co^{2+} and Ni^{2+} from single aqueous solution. Interestingly, cellulose modified with trimellitic anhydride (CTA) [8] exhibited a greater capacity to remove Co^{2+} and Ni^{2+} in comparison to SBSPh adsorbent. CTA is not a lignocellulose material and therefore does not contain components such as lignin and hemicelluloses, which are interfacing cellulose chains and can decrease the extent of a chemical modification. Moreover, due to the smaller particle size of cellulose in comparison to SB, cellulose has more accessibility to chemicals, thus allowing greater chemical modification and consequently higher adsorption capacity, but low applicability in real processes. In this study, it is noteworthy that the starting material (SB) is an important agroindustrial residue of the sugar and alcohol industry, presenting a low cost and a high availability. Therefore, its use as adsorbent is noble and environmentally friendly, reducing operating costs with the adsorptive process and making it economically viable for application in a wastewater treatment plant.

5. Conclusions

The one-pot synthesis of sugarcane bagasse cellulose mixed ester (SBSPh) was accomplished successfully, allowing the simultaneous introduction of different carboxylic acid groups (aliphatic and aromatic) onto sugarcane bagasse. The characterization of SBSPh material by ^{13}C Multi-CP solid-state NMR revealed that 0.33 succinyl units and 0.4 phthalyl units were introduced by cellobiose unity. Adsorption studies showed that the SBSPh adsorbent had an environmental applicability for

removal of Co^{2+} and Ni^{2+} from single aqueous solution. Adsorption kinetics for both metal ions were better described by the pseudo-second-order model. Equilibrium data were better described by the Sips model, suggesting heterogeneous adsorption of both metal ions on the SBSPh adsorbent. However, the presence of different carboxylic acids on the SBSPh surface did not result in selectivity for adsorption of Co^{2+} (Q_{max} = 0.53 mmol g^{-1}) and Ni^{2+} (Q_{max} = 0.49 mmol g^{-1}). Desorption and re-adsorption studies revealed that there were no significative losses in SBSPh adsorption capacity after one cycle of reuse of the adsorbent. Further studies will be performed with other ligands, such as trimellitic and pyromellitic anhydrides, to understand the role of the number of carboxylic groups in the aromatic unit in a more selective metal-ion adsorption.

Acknowledgments

The authors are grateful to Universidade Federal de Ouro Preto (UFOP) and Fundação de Amparo à Pesquisa do Estado de Minas Gerais (FAPEMIG grant number CEX-APQ-01287-15) for funding this research. Leandro V. A. Gurgel is grateful to Conselho Nacional de Desenvolvimento Científico e Technológico (CNPq grant number 305099/2016-7) for the fellowship awarded.

References

[1] C. Vaca-Garcia, M.E. Borredon, A. Gaseta, Determination of the degree of substitution (DS) of mixed cellulose esters by elemental analysis, Cellulose 8 (2001) 225-231.

[2] S. Kalia, L. Avérous, Biopolymers: biomedical and environmental applications, John Wiley & Sons, Inc., Hoboken, New Jersey, 2011.

[3] S. Possidonio, L.C. Fidale, O.A. El Seoud, Microwave-assisted derivatization of cellulose in an ionic liquid: An efficient, expedient synthesis of simple and mixed carboxylic esters, J Polym Sci Pol Chem 48 (2010) 134-143.

[4] T. Heinze, K. Rahn, M. Jaspers, H. Berghmans, p-Toluenesulfonyl esters in cellulose modifications: acylation of remaining hydroxyl groups, Macromolecular Chemistry and Physics 197 (1996) 4207-4224.

[5] C. Escudero-Oñate, N. Fiol, J. Poch, I. Villaescusa, Valorisation of lignocellulosic biomass wastes for the removal of metal ions from aqueous streams: A review, in: J.S. Tumuluru (Ed.) Biomass Volume Estimation and Valorization for Energy, InTech, Rijeka, 2017, pp. 381-407.

[6] M. Vandenbossche, M. Jimenez, M. Casetta, M. Traisnel, Remediation of heavy metals by biomolecules: A review, Crit. Rev. Env. Sci. Technol. 45 (2014) 1644-1704.

[7] T.A. Saleh, Advanced nanomaterials for water engineering, treatment, and hydraulics, IGI Global, Hershey, PA, 2017.

[8] F.S. Teodoro, S.N.d.C. Ramos, M.M.C. Elias, A.B. Mageste, G.M.D. Ferreira, L.H.M. da Silva, L.F. Gil, L.V.A. Gurgel, Synthesis and application of a new carboxylated cellulose derivative. Part I: Removal of Co^{2+}, Cu^{2+} and Ni^{2+} from monocomponent spiked aqueous solution, J. Colloid Interf. Sci. 483 (2016) 185-200.

[9] S. Afroze, T. Sen, M. Ang, Agricultural solid wastes in aqueous phase dye adsorption: A Review, in: C. Foster (Ed.) Agricultural wastes: Characteristics, Types and Management, USA: Nova Publishers, 2015, pp. 169-213.

[10] S. Hokkanen, A. Bhatnagar, M. Sillanpää, A review on modification methods to cellulose-based adsorbents to improve adsorption capacity, Water Res 91 (2016) 156-173.

[11] S.N.C. Ramos, A.L.P. Xavier, F.S. Teodoro, L.F. Gil, L.V.A. Gurgel, Removal of cobalt(II), copper(II), and nickel(II) ions from aqueous solutions using phthalate-functionalized sugarcane bagasse: Mono- and multicomponent adsorption in batch mode, Ind. Crop. Prod. 79 (2016) 116-130.

[12] S.N.d.C. Ramos, A.L.P. Xavier, F.S. Teodoro, M.M.C. Elias, F.J. Gonçalves, L.F. Gil, R.P. de Freitas, L.V.A. Gurgel, Modeling mono- and multi-component adsorption of cobalt(II), copper(II), and nickel(II) metal ions from aqueous solution onto a new carboxylated sugarcane bagasse. Part I: Batch adsorption study, Ind. Crop. Prod. 74 (2015) 357-371.

[13] B.E.L. Baêta, D.R.S. Lima, O.F.H. Adarme, L.V.A. Gurgel, S.F.d. Aquino, Optimization of sugarcane bagasse autohydrolysis for methane production from hemicellulose hydrolyzates in a biorefinery concept, Bioresour. Technol. 200 (2016) 137-146.

[14] D.R.S. Lima, O.F.H. Adarme, B.E.L. Baêta, L.V.A. Gurgel, S.F. de Aquino, Influence of different thermal pretreatments and inoculum selection on the biomethanation of sugarcane bagasse by solid-state anaerobic digestion: A kinetic analysis, Ind. Crop. Prod. 111 (2018) 684-693.

[15] J.S. Noh, J.A. Schwarz, Effect of HNO_3 treatment on the surface-acidity of activated carbons, Carbon 28 (1990) 675-682.

[16] S. Brunauer, P.H. Emmett, E. Teller, Adsorption of gases in multimolecular layers, J. Am. Chem. Soc. 60 (1938) 309-319.

[17] E.P. Barrett, L.G. Joyner, P.P. Halenda, The determination of pore volume and area distributions in porous substances. I. Computations from Nitrogen isotherms, J. Am. Chem. Soc. 73 (1951) 373-380.

[18] R.L. Johnson, K. Schmidt-Rohr, Quantitative solid-state 13C NMR with signal enhancement by multiple cross polarization, J. Magn. Reson. 239 (2014) 44-49.

[19] O.D. Bernardinelli, M.A. Lima, C.A. Rezende, I. Polikarpov, E.R. deAzevedo, Quantitative 13C MultiCP solid-state NMR as a tool for evaluation of cellulose crystallinity index measured directly inside sugarcane biomass, Biotechnol Biofuels 8 (2015) 110.

[20] G.C. Borgia, R.J.S. Brown, P. Fantazzini, Uniform-penalty inversion of multiexponential decay data, J. Magn. Reson. 132 (1998) 65-77.

[21] S.W. Provencher, CONTIN: A general purpose constrained regularization program for inverting noisy linear algebraic and integral equations, Computer Physics Communications 27 (1982) 229-242.

[22] Y.Q. Song, L. Venkataramanan, M.D. Hürlimann, M. Flaum, P. Frulla, C. Straley, T1–T2 correlation spectra obtained using a fast two-dimensional laplace inversion, J. Magn. Reson. 154 (2002) 261-268.

[23] C. Zhang, P. Li, Y. Zhang, F. Lu, W. Li, H. Kang, J.-f. Xiang, Y. Huang, R. Liu, Hierarchical porous structures in cellulose: NMR relaxometry approach, Polymer 98 (2016) 237-243.

[24] K.R. Brownstein, C.E. Tarr, Importance of classical diffusion in NMR studies of water in biological cells, Physical Review A 19 (1979) 2446-2453.

[25] D. Capitani, V. Di Tullio, N. Proietti, Nuclear magnetic resonance to characterize and monitor cultural heritage, Progress in nuclear Magnetic resonance Spectroscopy 64 (2012) 29-69.

[26] J. Mitchell, S.C. Stark, J.H. Strange, Probing surface interactions by combining NMR cryoporometry and NMR relaxometry, Journal of Physics D: Applied Physics 38 (2005) 1950.

[27] F.T.R.d. Almeida, B.C.S. Ferreira, A.L.d.S.L. Moreira, R.P.d. Freitas, L.F. Gil, L.V.A. Gurgel, Application of a new bifunctionalized chitosan derivative with zwitterionic characteristics for the adsorption of Cu^{2+}, Co^{2+}, Ni^{2+}, and oxyanions of Cr^{6+} from aqueous solutions: Kinetic and equilibrium aspects, J. Colloid Interf. Sci. 466 (2016) 297-309.

[28] R.A. Fideles, G.M.D. Ferreira, F.S. Teodoro, O.F.H. Adarme, L.H.M. da Silva, L.F. Gil, L.V.A. Gurgel, Trimellitated sugarcane bagasse: A versatile adsorbent for removal of cationic dyes from aqueous solution. Part I: Batch adsorption in a monocomponent system, J. Colloid Interf. Sci. 515 (2018) 172-188.

[29] S.Y. Lagergren, Zur theorie der sogenannten adsorption gelöster stoffe, kungliga svenska vetenskapsakademiens, Handlingar 24 (1898) 1-39.

[30] Y.S. Ho, G. McKay, Pseudo-second order model for sorption processes, Process Biochem. 34 (1999) 451-465.

[31] W.J. Weber, J.C. Morris, Kinetics of adsorption on carbon from solution, J. San. Eng. Div. 89 (1963) 31-60.

[32] G.E. Boyd, A.W. Adamson, L.S. Myers, The exchange adsorption of ions from aqueous solutions by organic zeolites. II. Kinetics, J. Am. Chem. Soc. 69 (1947) 2836-2848.

[33] D. Reichenberg, Properties of ion-exchange resins in relation to their structure. III. Kinetics of exchange, J. Am. Chem. Soc. 75 (1953) 589-597.

[34] I. Langmuir, The adsorption of gases on plane surfaces of glass, mica and platinum, J. Am. Chem. Soc. 40 (1918) 1361-1403.

[35] R. Sips, On the structure of a catalyst surface, J. Chem. Phys. 16 (1948) 490-495.

[36] O. Redlich, D.L. Peterson, A useful adsorption isotherm, J. Phys. Chem. 63 (1959) 1024-1024.

[37] M.M. Dubinin, L.V. Radushkevich, Equation of the characteristic curve of the activated charcoal, Proceedings of the National Academy of Sciences of the USSR, Physical Chemistry Section 55 (1947) 331-333.

[38] Y. Liu, Is the free energy change of adsorption correctly calculated?, J. Chem. Eng. Data 54 (2009) 1981-1985.

[39] L.V.A. Gurgel, M.T.B. Pimenta, A.A.d.S. Curvelo, Ethanol–water organosolv delignification of liquid hot water (LHW) pretreated sugarcane bagasse enhanced by high–pressure carbon dioxide (HP–CO_2), Ind. Crop. Prod. 94 (2016) 942-950.

[40] G.H. Mirzabe, A.R. Keshtkar, Application of response surface methodology for thorium adsorption on PVA/Fe_3O_4/SiO_2/APTES nanohybrid adsorbent, J. Ind. Eng. Chem. 26 (2015) 277-285.

[41] L.V.A. Gurgel, R.P. de Freitas, L.F. Gil, Adsorption of Cu(II), Cd(II), and Pb(II) from aqueous single metal solutions by sugarcane bagasse and mercerized sugarcane bagasse chemically modified with succinic anhydride, Carbohydr. Polym. 74 (2008) 922-929.

[42] D. Pavia, G. Lampman, G. Kriz, J. Vyvyan, Introduction to Spectroscopy, 4th ed., Cengage Learning, 2014.

[43] R. Łyszczek, Thermal and spectroscopic investigations of new lanthanide complexes with 1,2,4-benzenetricarboxylic acid, J. Therm. Anal. Calorim. 90 (2007) 533-539.

[44] A.K. Chandel, F.A. Antunes, M.B. Silva, S.S. da Silva, Unraveling the structure of sugarcane bagasse after soaking in concentrated aqueous ammonia (SCAA) and ethanol production by *Scheffersomyces* (*Pichia*) *stipitis*, Biotechnol Biofuels 6 (2013) 102.

[45] C.-F. Liu, R.-C. Sun, M.-H. Qin, A.-P. Zhang, J.-L. Ren, F. Xu, J. Ye, S.-B. Wu, Chemical modification of ultrasound-pretreated sugarcane bagasse with maleic anhydride, Ind. Crop. Prod. 26 (2007) 212-219.

[46] C.A. Rezende, M.A. de Lima, P. Maziero, E.R. deAzevedo, W. Garcia, I. Polikarpov, Chemical and morphological characterization of sugarcane bagasse submitted to a delignification process for enhanced enzymatic digestibility, Biotechnol Biofuels 4 (2011) 1-19.

[47] H.H. Wang, X.Q. Zhang, Y. Wei, C.F. Liu, Reaction behaviors of bagasse modified with phthalic anhydride in 1-Allyl-3-methylimidazolium chloride with catalyst 4-Dimethylaminopyridine, in: J.S. Tumuluru (Ed.) Biomass volume estimation and valorization for energy, InTech 2017, pp. 463-486.

[48] J.C.P. Melo, E.C. Silva Filho, S.A.A. Santana, C. Airoldi, Synthesized cellulose/succinic anhydride as an ion exchanger. Calorimetry of divalent cations in aqueous suspension, Thermochim. Acta 524 (2011) 29-34.

[49] J.C.P. Melo, E.C. da Silva Filho, S.A.A. Santana, C. Airoldi, Exploring the favorable ion-exchange ability of phthalylated cellulose biopolymer using thermodynamic data, Carbohyd Res 345 (2010) 1914-1921.

[50] W.M. Haynes, CRC Handbook of Chemistry and Physics, 95th ed., Taylor & Francis, 2014.

[51] K.A.G. Gusmao, L.V.A. Gurgel, T.M.S. Melo, L.F. Gil, Application of succinylated sugarcane bagasse as adsorbent to remove methylene blue and gentian violet from aqueous solutions - Kinetic and equilibrium studies, Dyes Pigm. 92 (2012) 967-974.

[52] R. Apiratikul, P. Pavasant, Batch and column studies of biosorption of heavy metals by *Caulerpa lentillifera*, Bioresour. Technol. 99 (2008) 2766-2777.

[53] J.-P.E. Grolier, J.M. del Río, Isothermal titration calorimetry: A thermodynamic interpretation of measurements, J. Chem. Thermodyn. 55 (2012) 193-202.

[54] A.L.P. Xavier, O.F.H. Adarme, L.M. Furtado, G.M.D. Ferreira, L.H.M. da Silva, L.F. Gil, L.V.A. Gurgel, Modeling adsorption of copper(II), cobalt(II) and nickel(II) metal ions from aqueous solution onto a new carboxylated sugarcane bagasse. Part II: Optimization of monocomponent fixed-bed column adsorption, J. Colloid Interf. Sci. 516 (2018) 431-445.

[55] S.N. do Carmo Ramos, A.L.P. Xavier, F.S. Teodoro, L.F. Gil, L.V.A. Gurgel, Removal of cobalt (II), copper (II), and nickel (II) ions from aqueous solutions using phthalate-functionalized sugarcane bagasse: mono-and multicomponent adsorption in batch mode, Industrial Crops and Products 79 (2016) 116-130.

[56] F.S. Teodoro, S.N. do Carmo Ramos, M.M.C. Elias, A.B. Mageste, G.M.D. Ferreira, L.H.M. da Silva, L.F. Gil, L.V.A. Gurgel, Synthesis and application of a new carboxylated cellulose derivative. Part I: Removal of Co 2+, Cu 2+ and Ni 2+ from monocomponent spiked aqueous solution, Journal of colloid and interface science 483 (2016) 185-200.

[57] P.X. Sheng, Y.-P. Ting, J.P. Chen, L. Hong, Sorption of lead, copper, cadmium, zinc, and nickel by marine algal biomass: characterization of biosorptive capacity and investigation of mechanisms, Journal of colloid and interface science 275 (2004) 131-141.

[58] V.C. Srivastava, I.D. Mall, I.M. Mishra, Competitive adsorption of cadmium (II) and nickel (II) metal ions from aqueous solution onto rice husk ash, Chemical Engineering and Processing: Process Intensification 48 (2009) 370-379.

[59] V.C. Srivastava, I.D. Mall, I.M. Mishra, Equilibrium modelling of single and binary adsorption of cadmium and nickel onto bagasse fly ash, Chemical Engineering Journal 117 (2006) 79-91.

Figure captions

Figure 1. Synthesis scheme used for preparation of sugarcane bagasse cellulose succinate phthalate (SBSPh) from sugarcane bagasse (SB) and succinic (SA) and phthalic (PA) anhydrides.

Figure 2. FTIR spectra of (a) SB and SBSPh and (b) SBSPh and SBSPh loaded with Co^{2+} (SBSPh-Co) and Ni^{2+} (SBSPh-Ni).

Figure 3. ^{13}C Multi-CP solid-state nuclear magnetic resonance spectra of SB and SBSPh.

Figure 4. Illustrative scheme of the chemical structure of SBSPh adsorbent considering the cellulose as the major component of raw SB modified with succinic and phthalic anhydrides (the numbers of succinyl and phthalyl units introduced into the SB structure quantified by ^{13}C Multi-CP solid-state nuclear magnetic resonance spectroscopy were 0.33 and 0.40 units per cellobiose unity (n = 1)).

Figure 5. T_2 distributions for SBSPh and SB samples. The solid black line is the distribution obtained from the ILT. The red, green and blue log-Gaussians describe the inner microfibril, cell wall and lumen interstitial spaces, respectively. In the inset, the plot the mean of the CPMG signals for the SB (red) and SBSPh (blue).

Figure 6. Effect of solution pH on the adsorption of Co^{2+} and Ni^{2+} on SBSPh adsorbent ($[M^{2+}]$ = 0.850 mmol L^{-1}, 25 °C, 130 rpm, t = 240 min, and 0.5 g L^{-1} SBSPh).

Figure 7. EDX images with surface mapping for (a) Co^{2+} and (b) Ni^{2+} adsorbed on the SBSPh adsorbent at 130 rpm, $[Co^{2+}]$ = 4.87 mmol L^{-1} and $[Ni^{2+}]$ = 3.22 mmol L^{-1}, 25 °C, and 0.5 g L^{-1} SBSPh.

Figure 8. Enthalpy of adsorption of Co^{2+} and Ni^{2+} as a function of the amount of metal ion adsorbed on the SBSPh surface at 25 °C.

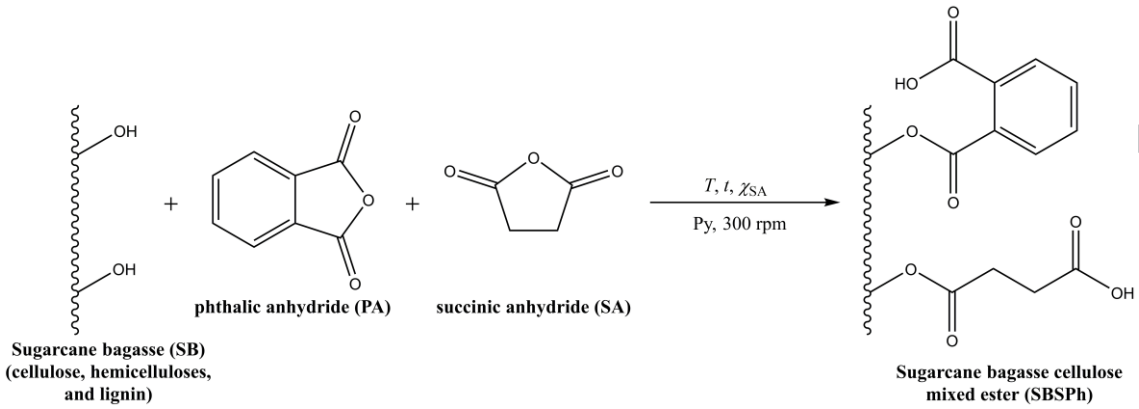

Sugarcane bagasse (SB) (cellulose, hemicelluloses, and lignin)

phthalic anhydride (PA)

succinic anhydride (SA)

Sugarcane bagasse cellulose mixed ester (SBSPh)

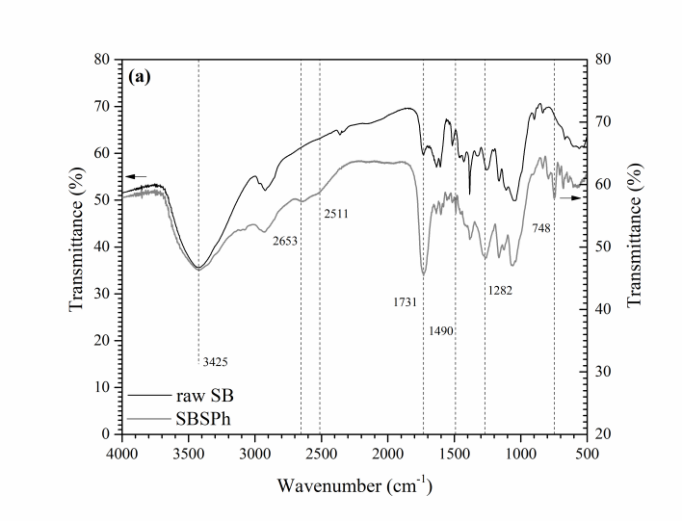

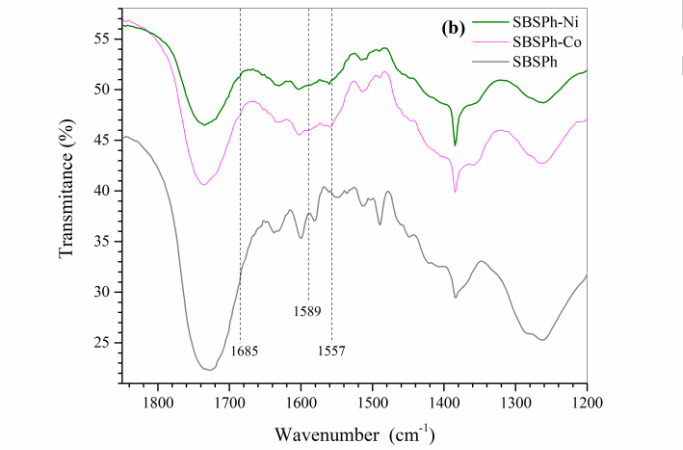

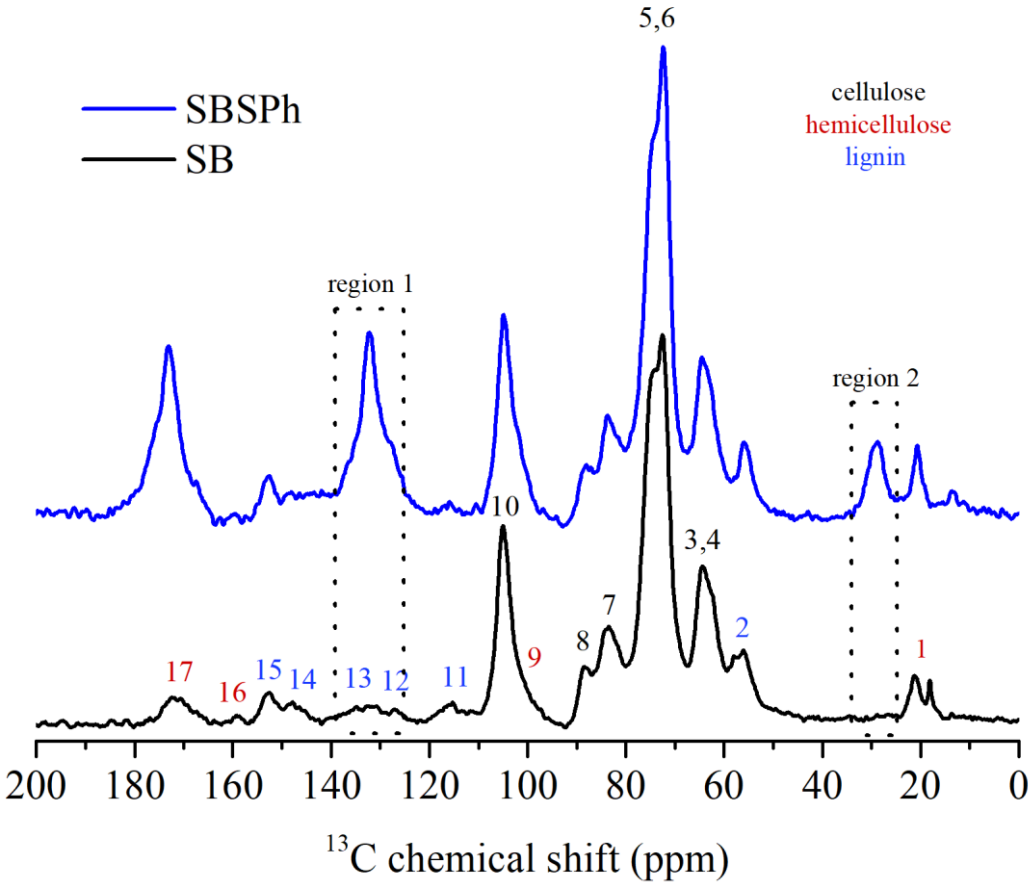

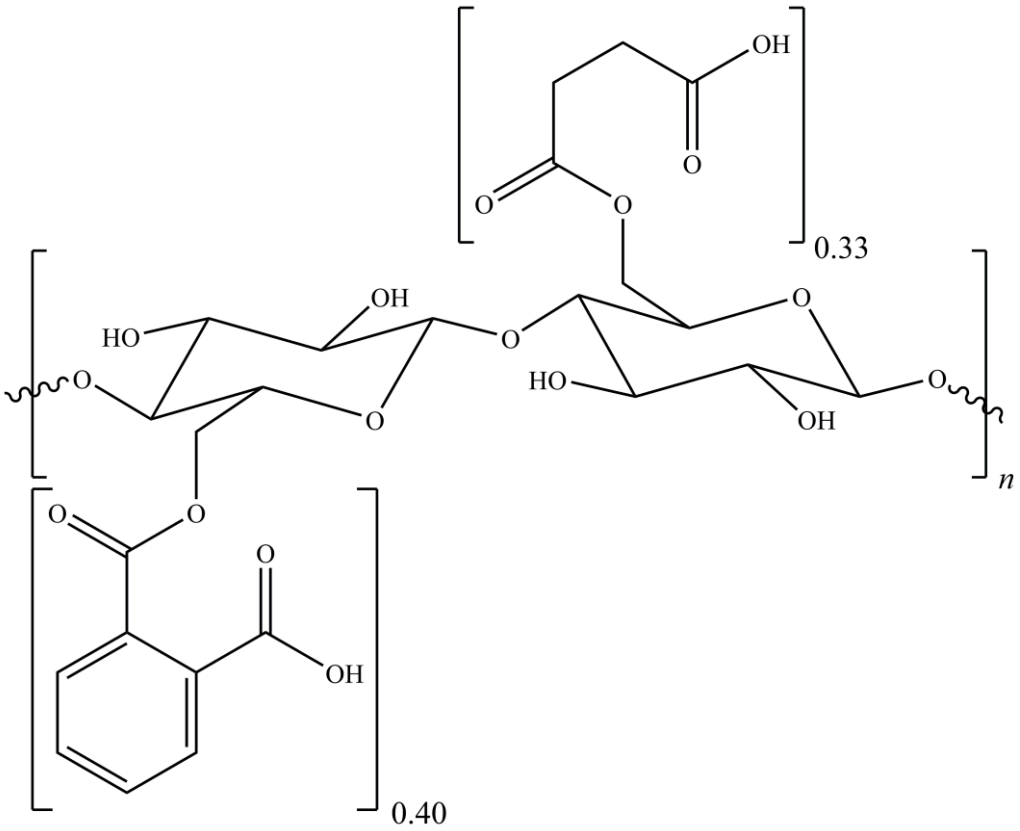

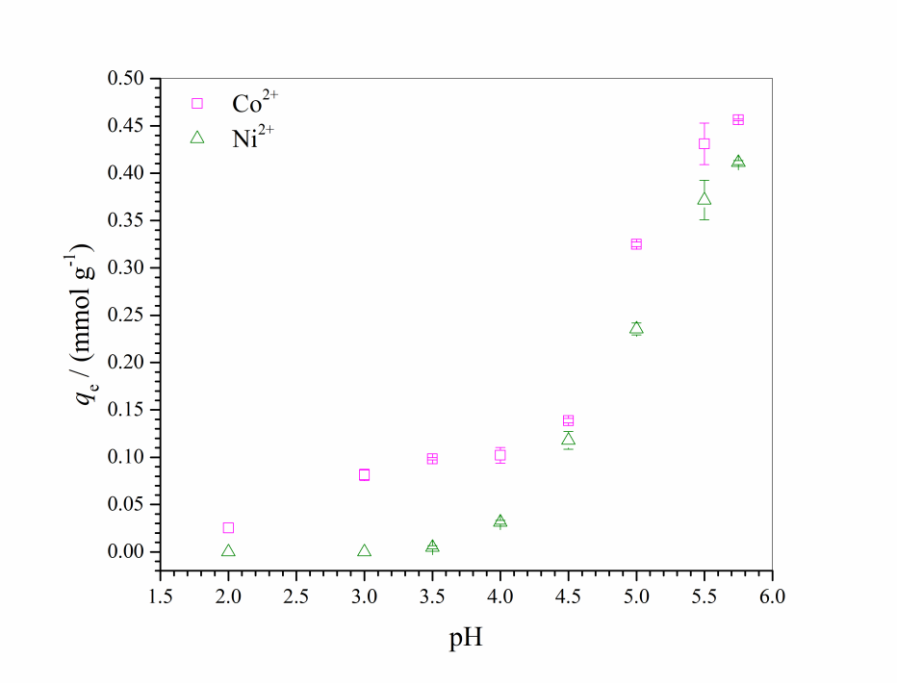

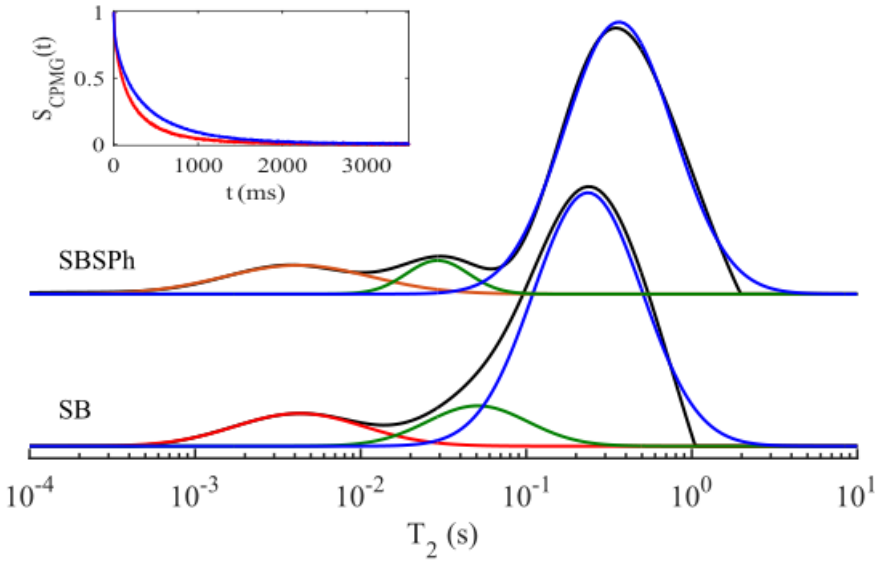

a)

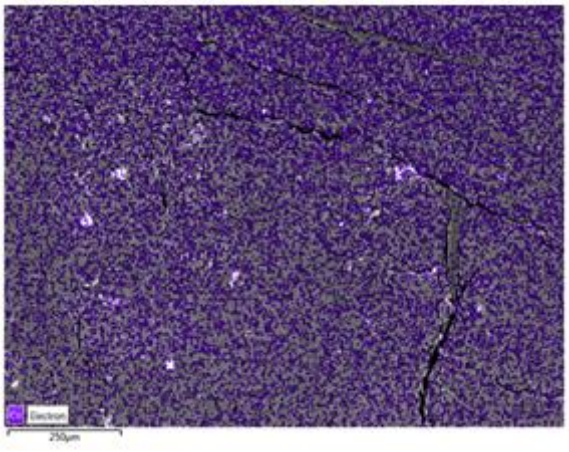

b)

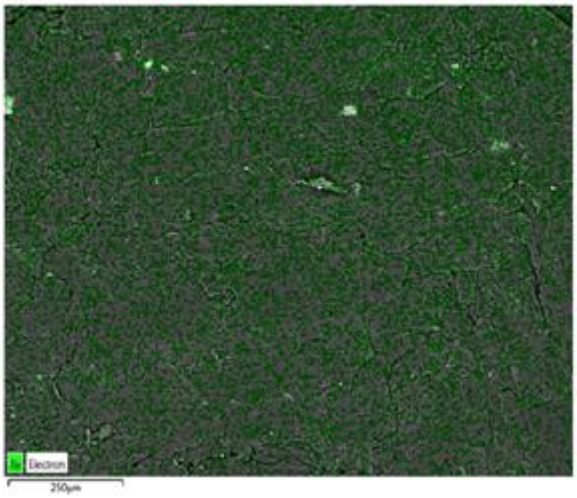

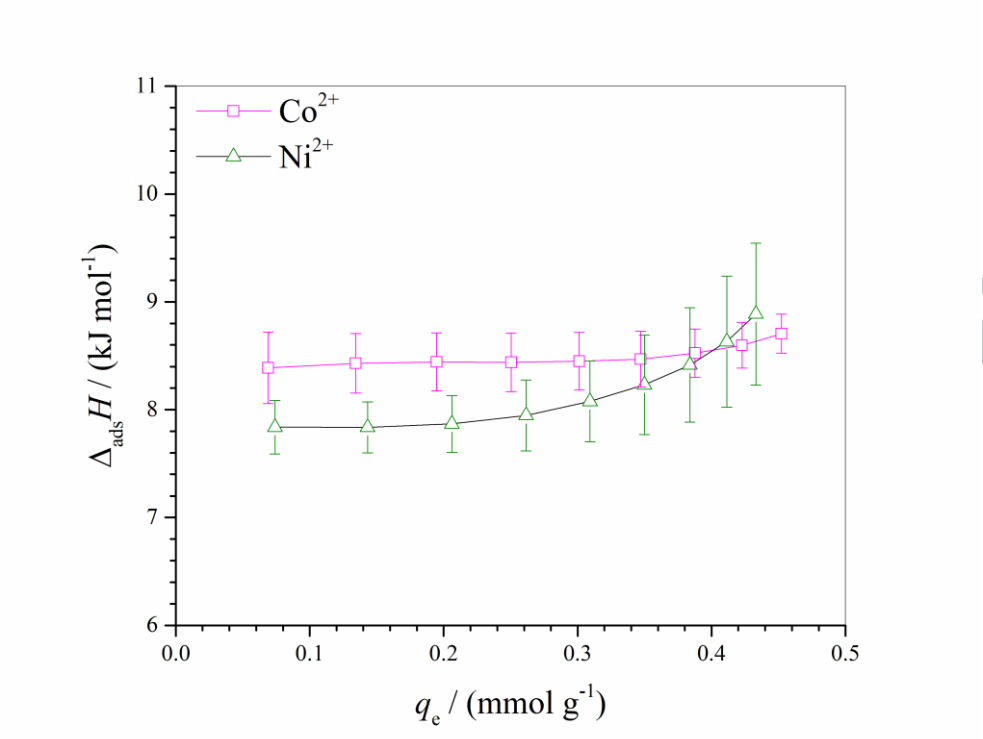

Table 1. 2^3 experimental design in terms of uncoded and coded variable levels and desired responses for evaluation of synthesis and application of sugarcane bagasse cellulose succinate phthalate for the removal of Co^{2+} and Ni^{2+} by adsorption.

Number of experiment	Independent variables							Dependent variables		
	Uncoded variables			Coded variables				Responses		
	T/(°C)	t/(min)	χ_{SA}	T/ (°C)	t/ (min)	χ_{AS}	wg/ (%)	$n_{T,COOH}$/ (mmol g^{-1})	$q_{Ni^{2+}}$/ (mmol g^{-1})	$q_{Co^{2+}}$/ (mmol g^{-1})
1	50	60	0.2	-1	-1	-1	25.03	1.70 ± 0.06	0.248 ± 0.000	0.259 ± 0.000
2	100	60	0.2	+1	-1	-1	54.39	2.94 ± 0.05	0.278 ± 0.000	0.280 ± 0.001
3	50	660	0.2	-1	+1	-1	43.01	4.83 ± 0.20	0.319 ± 0.000	0.310 ± 0.000
4	100	660	0.2	+1	+1	-1	59.07	3.41 ± 0.06	0.348 ± 0.000	0.346 ±0.000
5	50	60	0.8	-1	-1	+1	19.45	2.32 ± 0.03	0.203 ± 0.000	0.240 ± 0.000
6	100	60	0.8	+1	-1	+1	46.01	3.43 ± 0.07	0.264 ± 0.001	0.259 ± 0.000
7	50	660	0.8	-1	+1	+1	42.33	5.38 ± 0.02	0.317 ± 0.000	0.244 ± 0.000
8	100	660	0.8	+1	+1	+1	40.62	3.88 ± 0.03	0.330 ± 0.002	0.299 ± 0.000
9	75	360	0.5	0	0	0	50.64	3.87 ± 0.01	0.312 ± 0.000	0.336 ± 0.000
10	75	360	0.5	0	0	0	51.24	3.82 ± 0.02	0.308 ± 0.000	0.309 ± 0.001
11	75	360	0.5	0	0	0	52.50	3.92 ± 0.01	0.319 ± 0.000	0.308 ± 0.003

Table 2. Central T_2 values for each deconvoluted component in the T_2 distributions.

Sample	Inner microfibril /(s)	Cell Wall /(s)	Lumen /(s)
SB *in natura*	$(4.30 \pm 0.03) \times 10^{-3}$	$(4.98 \pm 0.01) \times 10^{-2}$	$(2.37 \pm 0.01) \times 10^{-1}$
SBSPh	$(4.1 \pm 0.4) \times 10^{-3}$	$(2.9 \pm 0.2) \times 10^{-2}$	$(3.43 \pm 0.03) \times 10^{-1}$

Table 3. Relative areas (%) for each deconvoluted component in the T_2 distributions and crystalline index.

Sample	Inner Microfibril /(%)	Cell Wall /(%)	Lumen /(%)
SB *in natura*	12 ± 1	10 ± 4	78 ± 4
SBSPh	12 ± 2	6 ± 2	82 ± 2

Table 4. Results of nonlinear (PFO and PSO) and linear (IPD and Boyd) regression analysis of the experimental kinetic data for adsorption of Co^{2+} and Ni^{2+} on the SBSPh adsorbent ($[M^{2+}]$ = 0.850 mmol L^{-1}, 25 °C, 130 rpm, pH 5.75, and 0.5 g L^{-1} SBSPh adsorbent).

Model	Parameter	Co^{2+}	Ni^{2+}
Experimental data	$q_{e,exp}$/(mmol g^{-1})	0.459 ± 0.007	0.470 ± 0.004
	t_e/(min)	180	120
Pseudo-first-order (PFO)	$q_{e,est}$/(mmol g^{-1})	0.437 ± 0.020	0.455 ± 0.011
	k_1/(min^{-1})	0.080 ± 0.015	0.058 ± 0.005
	R^2	0.767	0.973
	R^2_{adj}	0.753	0.972
	χ^2_{red}	0.009	0.003
Pseudo-second-order (PSO)	$q_{e,est}$/(mmol g^{-1})	0.455 ± 0.015	0.493 ± 0.012
	k_2/(g $mmol^{-1}min^{-1}$)	0.308 ± 0.058	0.156 ± 0.019
	R^2	0.899	0.980
	R^2_{adj}	0.892	0.978
	χ^2_{red}	0.004	0.002
Intraparticle diffusion (IPD)	*1st step*		
	$k_{i,1}$/(mmol g^{-1} $min^{-1/2}$)	$(3.6 \pm 0.4) \times 10^{-2}$	$(6.7 \pm 2.1) \times 10^{-2}$
	C/(mmol g^{-1})	$(1.3 \pm 0.1) \times 10^{-1}$	$(-1.8 \pm 6.1) \times 10^{-2}$
	R^2	0.957	0.832
	R^2_{adj}	0.948	0.748
	2nd step		
	$k_{i,2}$/(mmol g^{-1} $min^{-1/2}$)	$(2.1 \pm 0.8) \times 10^{-3}$	$(1.5 \pm 0.2) \times 10^{-3}$
	C/(mmol g^{-1})	$(4.2 \pm 0.1) \times 10^{-1}$	$(2.8 \pm 0.1) \times 10^{-1}$
	R^2	0.677	0.960
	R^2_{adj}	0.569	0.939
Boyd plot	B	$(2.11 \pm 0.18) \times 10^{-2}$	$(2.15 \pm 0.33) \times 10^{-2}$
	D_i/(m^2 min^{-1})	1.33×10^{-10}	1.36×10^{-10}

Table 5. Results of nonlinear regression analysis for modeling the equilibrium adsorption data with four isotherm models (25 °C, 130 rpm, pH 5.75, and 0.5 g L^{-1} SBSPh adsorbent).

Isotherm model	Parameter	Co^{2+}	Ni^{2+}
Experimental data	$q_{e,exp}$/(mmol g^{-1})	0.53 ± 0.00	0.49 ± 0.01
	t_e/(min)	180	120
	I_e/(mol L^{-1})	0.046	0.054
	γ_e	0.494	0.473
Langmuir	Q_{max}/(mmol g^{-1})	0.66 ± 0.02	0.54 ±0.01
	b/(L $mmol^{-1}$)	2.76 ± 0.17	4.66 ± 0.11
	R^2	0.993	0.999
	R^2_{adj}	0.993	0.999
	χ^2_{red}	1.1×10^{-3}	2.0×10^{-4}
	RSS	5.1×10^{-3}	1.2×10^{-3}
Sips	Q_{max}/(mmol g^{-1})	0.62 ± 0.02	0.53 ± 0.01
	b/(L $mmol^{-1}$)	3.31 ± 0.32	4.84 ± 0.18
	n	0.91 ± 0.05	0.97 ± 0.02
	R^2	0.995	0.999
	R^2_{adj}	0.994	0.999
	χ^2_{red}	9.0×10^{-4}	1.0×10^{-4}
	RSS	4.1×10^{-3}	1.0×10^{-3}
Redlich-Peterson (R-P)	K_R/(L g^{-1})	1.66 ± 0.15	2.38 ± 0.10
	a_R/(L $mmol^{-1}$)	2.40 ± 0.35	4.33 ± 0.25
	$Q_{max,est}$/(mmol g^{-1})	0.69 ± 0.12	0.55 ± 0.04
	β	1.00 ± 0.08	1.00 ± 0.02
	R^2	0.991	0.998
	R^2_{adj}	0.990	0.998
	χ^2_{red}	1.5×10^{-3}	3.0×10^{-3}
	RSS	7.9×10^{-3}	1.9×10^{-3}
Dubinin-Radushkevich (D-R)	$Q_{max,est}$/(mmol g^{-1})	0.53 ± 0.01	0.48 ± 0.01
	B/(mol^2 kJ^{-2})	0.04 ± 0.00	0.03 ± 0.00
	E/(kJ mol^{-1})	3.67 ± 0.04	4.18 ± 0.03
	R^2	0.985	0.993
	R^2_{adj}	0.984	0.992
	χ^2_{red}	2.4×10^{-3}	1.0×10^{-3}
	RSS	9.0×10^{-3}	3.5×10^{-3}

Table 6. Thermodynamic parameters for adsorption of Co^{2+} and Ni^{2+} on the SBSPh adsorbent at 298 K (25 °C).

Thermodynamic parameter /(kJ mol^{-1})	**Co^{2+}**	**Ni^{2+}**
$\Delta_{ads}G°$	-21.39 ± 0.76	-22.80 ± 0.25
$\Delta_{ads}H°$	8.43 ± 0.14	7.79 ± 0.11
$T\Delta_{ads}S°$	29.82 ± 0.77	30.59 ± 0.27

Table 7. 2^2 experimental design for efficiency of desorption (E_{des}) and efficiency of re-adsorption ($E_{re\text{-}ads}$) of Co^{2+} and Ni^{2+} for SBSPh adsorbent.

Number of experiment	**Independent variable**				**Dependent variable**			
	Uncoded values		**Coded values**		**Observed values**			
	C_{HNO_3}/ (mol L^{-1})	***t* (min)**	**C_{HNO_3}/ (mol L^{-1})**	***t* (min)**	**$E_{des,Co^{2+}}$/ (%)**	**$E_{re\text{-}ads,Co^{2+}}$/ (%)**	**$E_{des,Ni^{2+}}$/ (%)**	**$E_{re\text{-}ads,Ni^{2+}}$/ (%)**
1	0.010	5	-1	-1	49.33 ± 0.44	86.58	58.28 ± 4.86	100.09
2	1.000	5	+1	-1	67.28 ± 2.82	103.29	90.33 ± 7.20	119.55
3	0.010	45	-1	+1	79.86 ± 1.14	92.84	90.33 ± 0.37	107.85
4	1.000	45	+1	+1	83.29 ± 1.75	86.06	95.67 ± 5.02	100.15
5	0.505	25	0	0	71.86 ± 0.50	93.58	84.38 ± 0.84	109.20
6	0.505	25	0	0	73.01 ± 3.22	93.61	83.16 ± 0.93	109.24
7	0.505	25	0	0	72.72 ± 1.43	93.59	84.99 ± 0.28	109.19

Table 8. Comparison of SBSPh adsorbent for removal of Co^{2+} and Ni^{2+} from single aqueous solution with different adsorbent materials reported in the literature.

Adsorbent material	Metal ion	Q_{max}/ (mmol g^{-1})	pH	Particle size/ (mm)	Agitation/ (rpm)	Adsorbent dosage/ (g L^{-1})	Reference
Sugarcane bagasse modified with phthalic and succinic anhydride (SBSPh)	Co^{2+}	0.534[a]	5.75	0.500	130	0.5	This study
Sugarcane bagasse modified with phthalic anhydride (SPA)		0.462[a]	5.75	0.250	130	0.2	[57]
Raw sugarcane bagasse		0.064[a]	5.75	0.500	130	0.5	This study
Cellulose modified with trimellitic anhydride (CTA)		0.749[a]	5.5	0.250	130	0.2	[58]
Sugarcane bagasse modified with phthalic and succinic anhydride (SBSPh)	Ni^{2+}	0.494[a]	5.75	0.500	130	0.5	This study
Marine algal biomass *(Ulva* sp.).		0.290[b]	5.5	0.500-0.800	150	1.0	[59]
Marine algal biomass *(Gracillaria* sp.).		0.028[b]	5.5	0.500-0.800	150	1.0	[59]
Rice husk ash		1.4×10^{-3}[b]	6.0	0.150	150	10	[60]
Sugarcane bagasse ash		0.111[b]	6.0	<0.180-1.400	200	10	[61]
Raw sugarcane bagasse		0.089[a]	5.75	0.500	130	0.5	This study
Sugarcane bagasse modified with phthalic anhydride (SPA)		0.701[a]	5.75	0.250	130	0.2	[57]
Cellulose modified with trimellitic anhydride (CTA)		1.001[a]	5.5	0.250	130	0.2	[8]

[a] From equilibrium data; [b] From the Langmuir model.

Graphical abstract